

Integrating brain and biomechanical models - a new paradigm for understanding neuro-muscular control

Sebastian James^{1,2}, **Chris Papapavlou**⁵, **Alexander Blenkinsop**^{1,2},
Alexander Cope³,

Sean Anderson^{2,4}, **Konstantinos Moustakas**⁵, **Kevin Gurney**^{1,2,*}

¹ *Adaptive Behaviour Research Group, Department of Psychology, The University of Sheffield, Sheffield, UK*

² *Insigneo Institute for in-silico Medicine, The University of Sheffield, Sheffield, UK*

³ *Department of Computer Science, The University of Sheffield, Sheffield, UK*

⁴ *Department of Automatic Control Systems Engineering, The University of Sheffield, Sheffield, UK*

⁵ *Department of Electrical and Computer Engineering, The University of Patras, Patras, Greece*

Correspondence*:

Kevin Gurney

Department of Psychology, The University of Sheffield, Western Bank, Sheffield, S10 2TP, UK, k.gurney@sheffield.ac.uk

2 ABSTRACT

To date, realistic models of how the central nervous system governs behaviour have been restricted in scope to the brain, brainstem or spinal column, as if these existed as disembodied organs. Further, the model is often exercised in relation to an *in vivo* physiological experiment with input comprising an impulse, a periodic signal or constant activation, and output as a pattern of neural activity in one or more neural populations. Any link to behaviour is inferred only indirectly via these activity patterns. We argue that to discover the principles of operation of neural systems, it is necessary to express their behaviour in terms of physical movements of a realistic motor system, and to supply inputs that mimic sensory experience. To do this with confidence, we must connect our brain models to neuro-muscular models and provide relevant visual and proprioceptive feedback signals, thereby closing the loop of the simulation. This paper describes an effort to develop just such an integrated brain and biomechanical system using a number of pre-existing models. It describes a model of the saccadic oculomotor system incorporating a neuromuscular model of the eye and its six extraocular muscles. The position of the eye determines how illumination of a retinotopic input population projects information about the location of a saccade target into the system. A pre-existing saccadic burst generator model was incorporated into the system, which generated motoneuron activity patterns suitable for driving the biomechanical eye. The model was demonstrated to make accurate saccades to a target luminance under a set of environmental constraints. Challenges encountered in the development of this model showed the importance of this integrated modelling approach. Thus, we exposed shortcomings in individual model components which were only apparent when these

were supplied with the more plausible inputs available in a closed loop design. Consequently we were able to suggest missing functionality which the system would require to reproduce more realistic behaviour. The construction of such closed-loop animal models constitutes a new paradigm of *computational neurobehaviour* and promises a more thoroughgoing approach to our understanding of the brain's function as a controller for movement and behaviour.

Keywords: integrated brain biomechanics neuromuscular oculomotor saccade basal ganglia

1 INTRODUCTION

Note: Changes based on Reviewer 1's comments are in this colour. For Reviewer 2 we use this colour.

The field of computational neuroscience has provided many *systems models* of the brain (Arai et al., 1994; Gancarz and Grossberg, 1998; Hazy et al., 2007; Blenkinsop et al., 2017). We refer to these as *mechanistic computational models*, meaning models which consist of populations of neural elements, interconnected in a biologically plausible manner, which simulate the operation of the brain. Whilst they differ in scale and complexity, these models all seek to describe the fundamental mechanisms behind common animal behaviours such as locomotion, threat evasion, reaching or feeding. However, none of the models cited here actually reproduce these behaviours. In each case, the activity in a certain population of neurons is taken to be representative of a behavioural outcome. In some cases, it is reasonable to take the activity of an internal population within the brain model as being representative of the induced behaviour. For example, a choice made in a *go/no-go* task could be determined from activity in a population within a basal ganglia model (Nambu et al., 1990; Khn et al., 2004). The decision to *go* is selected by a reduction of activity in this population; maintenance of activity implies *no-go*. To validate the model, the error rates which it generates could be compared with experimentally determined error rates in primate subjects. We refer to this as an *output assumption model* because the output is assumed to signify behaviour. (An *input assumption model* assumes that sensory input produces some particular form of neural activity in an input population of the model.)

However, we may be interested in reproducing accurate simulated *trajectories*, in order to find out how degradation of parts of the model affect movement. In Parkinson's Disease, degradation of the dopamine neurons originating in the substantia nigra pars compacta (SNc) causes diskinesia (Galvan and Wichmann, 2008), as well as abnormal network activity in the basal ganglia (Brown et al., 2001; McCarthy et al., 2011). Sufferers of the disease would be expected to produce abnormal decision-making and movement trajectories in a reach-to-the-correct-target task such as the one described in James et al. (2017). A model which sought to explore in detail the effects of the SNc degradation both on the decision making and on the movement dynamics would need a physically accurate virtual arm, as well as physically realistic sensory input for the brain. This is no less than a complete model of those sections of the brain and body which act to fulfil the task. Such a modelling effort, if successful, would result in a virtual robot capable of expressing behaviour *in response to sensory input from its environment*. This would represent a paradigm shift in the field of computational neuroscience worthy of the new name of *computational neurobehaviour*.

In an attempt to build a model combining brain, realistic biomechanics and sensory feedback, we sought to extend our previous work modelling the oculomotor system by adding a virtual, biomechanical eye model able to make physically realistic movements. The rotational state of the eye would then determine how visual features in the virtual world were projected back into the brain model. The existing model (Cope et al., 2017) is already able to capture sensory input and convert it into a neural signal, assumed to specify the target of a *saccadic eye movement*; a fast movement of the eyes which directs the fovea to

64 a region of interest in the field of view. The oculomotor system is an excellent candidate for modelling
65 because its movements can be specified with only three degrees of freedom, making it one of the simplest
66 neuro-muscular systems in the body. It is nevertheless behaviourally interesting, as saccadic eye movements
67 reveal information about decision making at a subconscious level (Deubel and Schneider, 1996; Reppert
68 et al., 2015; Marcos and Genovesio, 2016). The modelling of the oculomotor system is served by a large
69 body of behavioural data describing saccades (Tipper et al., 2001; Walker et al., 1997; Casteau and Vitu,
70 2012), many anatomical studies of the neural substrates involved (Meredith and Ramoa, 1998; Isa, 2002;
71 Isa and Hall, 2009) and electrophysiological data linking these together (Hepp and Henn, 1983; Dorris et al.,
72 1997; McPeek et al., 2003; Vokoun et al., 2011). Furthermore, in the context of building *behaving* systems,
73 a necessary part of any model for which the behaviour requires visual attention and decision making is a
74 realistic mechanism for gathering visual information. This is obvious from extrinsic considerations—a
75 subject must look at a scene to make decisions or navigate within it. It also follows for *intrinsic* reasons.
76 For example, Howard and Tipper (1997) showed that visual cues affect reach trajectories and the same
77 group later demonstrated that reaching affects the saccadic system (Tipper et al., 2001) suggesting a close
78 relationship between these neural systems. **Building a behaving oculomotor system will therefore assist**
79 **future computational neurobehavioural modelling efforts that involve reaching.**

80 Many neural populations are involved in the coding of saccadic eye movements, only a very brief
81 overview is given here; for a review, see Munoz (2002). One pathway takes information from the retina
82 directly into the superficial layers of the superior colliculus in the brainstem (Sterling, 1971; Linden and
83 Perry, 1983; Wu et al., 1994). Activity within the superior colliculus then excites neurons in the pons,
84 medulla and rostral mid-brain (Sparks, 2002). and **finally the motor neurons** which innervate the extraocular
85 muscles (Fuchs and Luschei, 1970; Sparks, 2002). This direct pathway is responsible for the low latency
86 saccades called express saccades (Schiller et al., 1987; Edelman and Keller, 1996). Information from the
87 retina is also processed by visual cortex which feeds through to the frontal eye fields in which activity is
88 related to reflexive and voluntary saccades (Schall and Thompson, 1999). Activity build-up in the frontal
89 eye fields is transferred to the intermediate layers of the superior colliculus (Stanton et al., 1988b) and is
90 also processed by the basal ganglia, which participates in the selection of the winning saccade end point
91 (Stanton et al., 1988a; Hikosaka et al., 2000). Although both cortical and subcortical paths produce a
92 saccade target signal in the superior colliculus, it is also possible for animals to make relatively normal
93 saccades even after the colliculus has been ablated (Wurtz and Goldberg, 1972; Aizawa and Wurtz, 1998),
94 though express saccades are lost with collicular lesions (Schiller et al., 1987). This makes the superior
95 colliculus a perplexing structure, being both critically involved in saccade target specification (Sparks and
96 Nelson, 1987) and saccade dynamic control (Waitzman et al., 1991; Goossens and van Opstal, 2012) and
97 yet dispensable. The ‘backup pathway’ likely incorporates the oculomotor vermis and fastigial oculomotor
98 region of the cerebellum which are known to participate in the specification, dynamics and adaptation of
99 saccadic eye movements (Kleine, 2003; Takagi et al., 1998).

100 There is a long history of modelling the oculomotor system. For a comprehensive review, see Girard and
101 Berthoz (2005). Models of individual **sub-systems** have been proposed for brainstem (Robinson, 1975;
102 Scudder, 1988; Gancarz and Grossberg, 1998), cerebellum (Quaia et al., 1999; Dean, 1995; Dean et al.,
103 1994) and superior colliculus (Massone, 1994; Arai et al., 1994; Morén et al., 2013; Marino et al., 2012).
104 More recently, combined models have also been developed incorporating sensory input (Cope et al., 2017)
105 and driving **a second order differential equation** representing the eye (Tabareau et al., 2007; N’Guyen
106 et al., 2014; Thurat et al., 2015). None of these models has yet fully closed the loop to produce a behaving
107 system operating freely within its environment. We argue that developing integrated, closed-loop models of

108 behaving systems offers insights into the operation of neural systems that are not available from input- or
109 output-assumption models.

2 MATERIAL & METHODS

110 The integrated brain and biomechanical model described here is a development of the model in Cope
111 et al. (2017), referred to here as the Cope-Chambers model. This was a rate-coded neural network model
112 incorporating retinal populations, frontal eye fields (FEF), the basal ganglia (BG), and the superior colliculus
113 (SC). The Cope-Chambers model takes as *input* the positions of luminances (of fixed shape and intensity)
114 on a topographic map. Whilst certain assumptions were made about the input—that a luminant input excites
115 activity on a retinotopic layer, with computer code carrying out the transformation achieved in the brain by
116 a neural connectivity map (Thivierge and Marcus, 2007)—it is nonetheless *not* an input-assumption model
117 according to our definition because the activity generated in the neural input layer is modelled as a response
118 to the luminances, rather than being crafted. In the Cope-Chambers model, the centroid of the activity in
119 the deep layers of superior colliculus was assumed to accurately encode the location of the eye at the end
120 of the saccade (Wurtz and Goldberg, 1972; Robinson, 1972; Van Gisbergen et al., 1987; McIlwain, 1982).
121 This location was used to recalculate the positions of the luminances in the eye's frame of reference at each
122 time step. Because a pattern of neural activity in the output population was assumed to have a behavioural
123 outcome, it was thus an *output-assumption model*. The model included no brainstem populations other
124 than superior colliculus, nor a neuromuscular model.

125 To the Cope-Chambers model, we added a brainstem model and a biomechanical eye model. The rate-
126 coded brainstem model was taken from the literature (Gancarz and Grossberg, 1998) as the best-of-breed
127 saccadic burst generator (Girard and Berthoz, 2005). The biomechanical eye was implemented using the
128 biomechanical modelling framework OpenSim; the brain and brainstem were modelled using the SpineML
129 toolchain. These will be described below, along with a review of the Cope-Chambers model, but first we
130 will give a description of the co-ordinate systems.

131 2.1 Co-ordinates in the world

132 Before describing the biomechanical eye and the brain model, which consisted of retinotopically mapped
133 neural sheets, we describe the co-ordinate system used in the world. The eye was located at the origin of a
134 three-dimensional, right-handed Cartesian co-ordinate system, with its fovea directed in the $-z$ direction.
135 There was a notional spherical screen which was also centred at the origin of the co-ordinate system and
136 had a radius of 50 (in arbitrary units). The *fixation point* was the point on the screen at which the eye
137 was initially directed. Onto the screen were projected target luminances, each of which having a position
138 described by two co-ordinates; θ_x^t , a rotation of the horizon plane about the x axis, and θ_y^t , a rotation of the
139 meridian plane about the y axis. The position is the intersection of these rotated planes with the spherical
140 screen (disregarding the intersection point of these three surfaces behind the eye). Note that a luminance
141 with positive θ_x^t was above the horizon of this world; one whose θ_y^t was positive lay to the left of the
142 world's meridian. For this reason, many of the figures in this paper are plotted with $-\theta_y$ on the x -axis and
143 θ_x on the y -axis so that targets that lay up and to the right in the world do so in the graphs, also.

144 Luminances were crosses of height and width subtending $\pm 3^\circ$ and whose 'bars' were 2° thick. Lumi-
145 nances were oriented like + symbols with their vertical bar aligned with the meridian plane and their
146 horizontal bar aligned with the horizon.

147 The eye's frame of reference was initially aligned with the world's frame of reference. At each timestep,
148 the eye's rotational state (described by the Euler rotations θ_x , θ_y , θ_z) was used to translate the three
149 dimensional Cartesian co-ordinates of the luminances in the world frame into co-ordinates in the eye frame.
150 The luminance co-ordinates in the eye's frame of reference were used to determine the input to the brain
151 model.

152 2.2 Existing brain model

153 The brain model, excluding the brainstem, is a re-implementation of the Cope-Chambers model, of
154 reflexive saccadic behaviour (Cope et al., 2017). Reflexive saccades are fast eye movements elicited by
155 abrupt changes in the peripheral visual scene (reflexive saccades can occur also as a result of auditory
156 and somatosensory stimuli, but these modalities are ignored in this model). A reflexive saccade has a
157 starting position defined by the initial orientation of the eye and an end-point position in which the eye
158 is directed towards a new target. Regardless of the number of targets within the visual scene, the brain
159 must choose one location as the end-point, because the eyes can look only in one direction at a time. The
160 functionality reproduced by the Cope-Chambers model is 'the selection of the best target end-point for
161 a reflexive saccade'. A competition such as this between incompatible movements is often referred to
162 as an *action selection* problem (Norman and Shallice, 1986; Maes, 1989; Redgrave et al., 1999). The
163 Cope-Chambers model is therefore a model of action-selection in the oculomotor system for reflexive
164 saccades. One hypothesis for the rôle played by the basal ganglia (BG) is that the system performs *action*
165 *selection* (Mink, 1996; Redgrave et al., 1999; Hikosaka et al., 2000). The Cope-Chambers model places the
166 BG at the centre of the oculomotor system; this follows the known anatomy of the region (Hikosaka et al.,
167 2000) and provides a mechanism for action selection of the best saccade. The BG receives input indirectly
168 from the superior colliculus, which has a retinotopic arrangement (Ottos et al., 1986).

169 The BG receives excitatory inputs directly from retinotopic regions of the cortex including the frontal eye
170 fields (FEF), supplementary eye fields (SEF), lateral intraparietal cortex (LIP) and dorsolateral prefrontal
171 cortex. The dorsolateral prefrontal cortex, which participates in voluntary saccades (Funahashi et al., 1993;
172 Munoz and Everling, 2004), is not modelled because the model concerns reflexive rather than voluntary
173 eye movements. Several other regions of the brain that are associated with eye movements are also omitted
174 from the model. The early visual processing stream in cortex, from V1, through to the LIP is subsumed into
175 a 'sustained retinal' signal which arrives at FEF. The justification here is that the model reacts to simple
176 luminant targets and does not need to carry out the feature extraction performed by these visual areas. The
177 supplementary eye fields are involved in the programming of saccade sequences (Tehovnik et al., 2000)
178 and memory guided saccades (Chen and Wise, 1995; Schlag, 2002). Lesions of SEF do not affect visually
179 guided saccades (Gaymard et al., 1998) and so the SEF is also omitted from the model.

180 Fig. 1(a) shows the macroscopic architecture of the Cope-Chambers model. The figure shows the
181 relationships between the retinal input populations, the FEF, the populations comprising the BG sub-system
182 (the red border indicates that the box represents a number of populations as a sub-system), the thalamus and
183 the superior colliculus. Excitatory connections are indicated with arrow heads; inhibitory connections with
184 circles in place of the arrow heads. The blue and green connection lines indicate two thalamo-basal ganglia
185 loops, one cortical loop through FEF (green), the other a sub-cortical loop through SC. It is important to
186 note that although they are given different colours in the diagram, these loops are in no way independent,
187 with loop activity combining both in thalamus and in the basal ganglia and a direct excitatory, feed-forward
188 connection from FEF to SC.

189 The basal ganglia sub-system is the most complex component of the Cope-Chambers model. The BG
190 model is based on previous work (Gurney et al., 2001b,a) and is referred to as the GPR model. The GPR model
191 incorporates the following main components of the primate BG (Mink, 1996; Wickens, 1997): (i)
192 The striatum (the main input station to the BG) which is divided into two iterdigitated populations of
193 projection neurons expressing primarily D1 or D2-type dopaminergic receptors (named Str_D1 and Str_D2);
194 (ii) The subthalamic nucleus (STN); (iii) the external segment of the globus pallidus (GPe); (iv) the output
195 nucleus relevant for saccadic control—the substantia nigra pars reticulata (SNr) (Hikosaka et al., 2000).

196 The connectivity of the GPR model [Fig. 1(b)] is constrained by the known anatomy and physiology of
197 the BG (Bolam et al., 2000). Physiologically, the only source of glutamate within the BG is the STN, whose
198 projections are therefore excitatory; all other nuclei have GABAergic projection neurons and are therefore
199 inhibitory. The cortex sends glutamatergic projections to both the Str_D1 striatal population, which projects
200 preferentially to the SNr, and to Str_D2, which projects primarily to GPe (Gerfen et al., 1990). The cortex
201 also projects to the STN, which sends diffuse projections to the SNr and GPe (Parent and Hazrati, 1993).
202 The GPe projects to the SNr and also projects back to the STN, completing a GPe-STN loop.

203 The GPR model is arranged into ‘action channels’; Fig. 1(b) shows an example network containing three
204 channels. It is between these channels that competition occurs, with the winning channel succeeding in
205 reducing activity in the output nucleus, SNr, and thereby disinhibiting its target. The complete connectivity
206 pattern for this small network is shown in Fig. 1(b); the left channel in cortex innervates the left channels
207 of Str_D1, STN and Str_D2. Connections are one-to-one, so it follows that the middle channel of cortex
208 innervates the middle channels of STN and the striatal populations and the right channel of cortex innervates
209 right channels in striatum and STN. Striatal population channels also inhibit SNr and GPe on a one-to-one
210 basis and GPe feeds inhibition to SNr and STN in a one-to-one manner. The outputs from STN however
211 are not one-to-one. The output from all channels of STN is summed together and then the sum is fed into
212 each channel of SNr and GPe. This models the diffuse excitation from STN which has been observed in
213 the BG (Parent and Hazrati, 1993).

214 Within the BG, there are several mechanisms supporting competitive processing for selecting channels
215 whose inhibitory output should be reduced. The selection mechanism of the GPR model is the ‘off-centre,
216 on-surround’ scheme proposed by Mink and Thach (1993). The ‘on-surround’ is provided by diffuse,
217 excitatory projections from the STN to the SNr. Focussed inhibition from the Str_D1 neurons in striatum
218 contributes the ‘off-centre’ part of the mechanism. This arrangement leads to selection behaviour via a
219 release of target inhibition, since channels that have strong salience (input) have weak output at the level of
220 SNr, and channels with weak salience have enhanced output.

221 The GPe is not included in the centre-surround circuit described above, but still plays a key rôle in
222 selection. Operating alone, the Str_D1/STN/SNr circuit can suffer from the following problem: if the input
223 for all channels is relatively high, then the diffuse projection from STN, which effectively supplies a sum
224 of *all* of the STN inputs to each channel in SNr, will provide so much excitation that Str_D1 may become
225 unable to inhibit one of the channels in SNr and selection may become impossible. Gurney et al. (2001b,a)
226 showed that the inhibitory feedback from GPe to STN acts as an ‘automatic gain control’ to help prevent
227 this from occurring.

228 At the neuronal level, the STN, GPe and SNr have tonic output levels (Chevalier and Deniau, 1990;
229 DeLong et al., 1985; Kita and Kitai, 1991). This is modelled using piecewise linear output functions
230 with zero offsets, c (see Eq. 6) but with noise added to the input. In striatum, Str_D1 and Str_D2 have
231 positive offset c , mimicking the so-called ‘down-state’ of medium spiny neurons which have a resting

232 potential far below spiking threshold and require co-ordinated input to generate action potentials (Wilson
 233 and Kawaguchi, 1996). In addition, the Str_D1 and Str_D2 neurons are influenced by dopamine in different
 234 ways; facilitating cortico-striatal transmission at medium spiny neurons with D1 receptors (Hernndez-Lpez
 235 et al., 1997; Gonon, 1997) and reducing transmission at those with D2 receptors (Delgado et al., 1999).
 236 These effects are modelled using a dopamine parameter, d , which modulates the input activations a_{in}^{D1} and
 237 a_{in}^{D2} as:

$$a_{in}^{D1} = (0.2 + d)A \quad (1)$$

$$a_{in}^{D2} = (1 - d)A \quad (2)$$

238 where A is the input activation (see also Eqns. 10 & 11). For the ‘normal, healthy’ value for d of 0.7,
 239 Str_D1 activation is relatively enhanced ($0.9A$); Str_D2 activation is one third of this value ($0.3A$). The
 240 major effect of this difference in the relative strength of the activity in Str_D1 versus Str_D2 is simply that
 241 a change in the level of activity in Str_D1 affects the off-centre, on-surround mechanism. The effect of
 242 varying the input into Str_D2 is much more subtle, with only a small change in the amount of inhibition fed
 243 from GPe into STN (via a focussed, one to one connection) being affected by the change, along with a
 244 small change in the inhibition fed into SNr from GPe (also via a one to one connection). It is not possible
 245 to clearly describe the dynamic effect of the dopamine parameter as being due to any single population,
 246 because the activity is recurrently connected through multiple loops. Thus, a line of reasoning such as
 247 “reduced activity for a luminance in Str_D2 will lead to less inhibition in that region in GPe, which means
 248 that there will be higher activity there, and hence more inhibition for that region passed to STN leading us
 249 to expect less activity in STN” is verified by running a suitable simulation with the model, but the effect is
 250 small. Note that the effect of dopamine in the model is only to modulate the strength of cortico-striatal
 251 synapses; no learning is modelled and so the significance of dopamine as a prediction error signal is outside
 252 the scope of the current work.

254 The GPR model in Fig. 1(b) has only three channels, with the focussed inhibition from striatum to SNr
 255 and GPe defined by a simple one-to-one scheme. The action channels represent discrete, incompatible
 256 motor action choices. In the oculomotor model, an action channel represents the end-point of saccade,
 257 and the competition carried out in the basal ganglia is between potential saccade end-points. However,
 258 eye movements have a *continuous* end-point space; the eye can rotate to any orientation within its
 259 biomechanically permissible range. Some end-points within this range are mutually exclusive—it’s not
 260 possible to look to the left and to the right simultaneously—but *nearby* end-points are not necessarily
 261 incompatible. A small enough error in the end-point of a saccade will not prevent the eye from foveating on
 262 a target as the foveal region of high visual acuity is not infinitesimally small. To cope with this requirement,
 263 the populations within the oculomotor basal ganglia are conceived of as two-dimensional topographic
 264 grids of leaky integrator neural elements. Activity in each element corresponds to a spatial location in the
 265 visual field. Neighbouring elements correspond to locations which are close to each other in the visual field.
 266 Focussed one-to-one projections in the GPR model are replaced by projective fields with many weighted
 267 connections. Specifically, each unit in Str_D1 projected to a counterpart SNr_j in SNr with some weight
 268 w_{max} , but also connected to neighbouring nodes in SNr with a weight given by $w_{max} \cdot G(d)$, where $G(d)$ is
 269 a circularly symmetric, 2D-Gaussian which is a function of distance d from SNr_j [Fig. 1(c)]. A similar
 270 scheme applied for the connectivity from Str_D2 to GPe and for a number of the other connections in the
 271 Cope-Chambers model; in the SpineML implementation of the model, this connectivity scheme is named
 272 ‘GaussianKernel’. Fig. 2 shows a schematic of the SpineML implementation of the model, based on a
 273 diagram output directly from SpineCreator. Populations for Str_D1, Str_D2, STN, SNr and GPe are shown
 274 within the ‘Basal Ganglia’ box. Input comes into the model via the ‘World’ population and the output

275 population is SC_deep. Compare this diagram with Figs. 1(a) & (b). Fig. 2 expands the ‘SC’, ‘BG’ and
276 ‘slow retinal’ boxes from Fig. 1(a).

277 The frontal eye fields (FEF) are a key cortical area for the generation of saccadic eye movements (Hikosaka
278 et al., 2000; Tehovnik et al., 2000; Robinson and Fuchs, 1969; Bruce and Goldberg, 1985). Saccadic targets
279 are mapped retinotopically over its surface (Robinson and Fuchs, 1969; Bruce and Goldberg, 1985; Sabes
280 et al., 2002), and increased neural activity at a location in the map precedes a saccade to that location.
281 Importantly, the FEF is also associated with visual decision making (Thompson and Bichot, 2005; Schall
282 et al., 1995; Monosov et al., 2008; Cohen et al., 2009). Thus, in a saccade choice, increased FEF activity is
283 predictive of the eye movement whether correct or incorrect (Thompson et al., 2005), rather than of the
284 correct response.

285 FEF neurons can be divided in to three functional groups, related to whether their activity corresponds
286 with visual stimuli, motor action, or both (Segraves and Goldberg, 1987). The Cope-Chambers model
287 simplifies this categorisation using a single layer of 50 by 50 units representing the mean of all three
288 groups. This layer therefore responds to both visual stimuli and the buildup of activity associated with
289 motor (saccadic) action. The retina provides a persistent luminance signal into the FEF through the dorsal
290 visual pathway (Ungerleider and Mishkin, 1982) which is abbreviated in this model to a direct connection
291 with delay.

292 The FEF provides input into the BG (Saint-Cyr et al., 1990) (to Str_D1, Str_D2 and STN) which, in turn,
293 projects back to thalamus in a retinotopically organised way (Middleton and Strick, 2000; Lynch et al.,
294 1994). In addition, the thalamic targets of this path are regions with strong reciprocal connections to the
295 FEF (McFarland and Haber, 2002). In this way, the FEF forms channel-based loops through basal ganglia
296 of the kind described above. Such circuits formed the basis of the model of Humphries and Gurney (2002).
297 The thalamo-cortical loop may be thought of as an integrator of information, whose gain is modulated by
298 inhibition from basal ganglia (Chambers et al., 2012; Cope and Gurney, 2011).

299 The superior colliculus (SC) is a sub-cortical nucleus which also plays a critical rôle in the generation
300 of saccades (Hikosaka and Wurtz, 1983). Both FEF and SC have direct connections to the saccadic burst
301 generator (SBG, see Sect. 2.3). If either is lesioned, the other can direct gaze, following a period of
302 adjustment (Latto, 1977), albeit with some persistent deficits. The SC is also a direct target of output
303 from the SNr (Jayaraman et al., 1977; Jiang et al., 2003) and can be influenced by the action selection
304 mechanisms of the BG. In particular, it forms a loop with BG, but unlike its cortical counterpart in FEF, the
305 input to basal ganglia comes via the thalamus [Fig 1(a), blue arrows].

306 While the SC has seven alternating cell- and fibre-rich layers (Wurtz and Albano, 1980), in most
307 cases these are divided into the ‘superficial’ and ‘deep’ layers, which have significantly different response
308 properties. Cells in the superficial layers, which receive input from the retina, are mainly visually responsive,
309 with a preferred response to phasic events (luminance onsets and offsets) and movement on the visual
310 field (Goldberg and Wurtz, 1972). In contrast, cells in the deep layers receive multi-modal input, including
311 inhibitory input from the output structures of the BG (Jayaraman et al., 1977), and are directly involved
312 in the generation of saccadic eye movements. Saccade related activity in the deep layers appears to
313 generate saccades through ‘population coding’, with a weighted sum of activity across the retinotopy of SC
314 determining the saccade target (Lee et al., 1988; van Opstal and van Gisbergen, 1990; Mays and Sparks,
315 1980). The deep layers of SC receive input from the FEF in a topographic manner (Stanton et al., 1988a;
316 Sommer and Wurtz, 2000).

317 The SC in the Cope-Chambers model is based on the the model described in Arai and Keller (2005), with
318 the difference that the SNr input to the SC is generated by the BG model, rather than being hand-crafted.
319 The SC model has a superficial and a deep layer, each of which is a 2-D array of 50 by 50 leaky integrator
320 units arranged in the same retinotopic manner as the FEF (Wurtz and Albano, 1980).

321 The Cope-Chambers model incorporates a special connectivity pattern for visual input via cortical (FEF)
322 and sub-cortical (thalamus) pathways. Due to the retinotopic mapping (Sect. 2.2.2), foveal luminances
323 deliver a strong signal to the BG; roughly one third of the map is activated for the foveal targets used in
324 this work (Fig. 3, red cross). This makes it virtually impossible for a peripheral target (Fig. 3, yellow cross)
325 to win selection in the BG. Even if the peripheral target competed successfully to generate a saccade, this
326 process would cause a significant delay, leading to latencies much larger than those observed experimentally.
327 To overcome this problem, the Cope-Chambers model incorporates a mechanism in which the synaptic
328 strength of connections between FEF, thalamus and striatum are reduced close to the fovea according to a
329 shifted hyperbolic tangent. This connection is named ‘DecayingAtFovea’ in the SpineML implementation
330 and follows a modified sigmoidal curve rather than tanh. In either case, the relation is ‘S-shaped’ and
331 normalised to the range [0 1]. Far from the fovea (where the S-shaped curve has the value ≈ 1), the
332 connectivity pattern looks almost identical to a one-to-one connection.

333 Input to the Cope-Chambers model is provided through a simple retina model which directly samples
334 from a larger ‘world array’ of pixel values. In the current model, the input for the retina is named ‘World’
335 and is the retinotopic projection [Fig. 2(b)] of the eye’s field of view of the world [Fig. 2(a)] and the
336 luminant targets therein. The raw input in ‘World’ is fed into a population which adds noise, and then
337 via a delayed connection to FEF (the sustained retinal input path), to simulate processing through the
338 dorsal visual stream. It is also fed, without substantial delay, into two leaky integrator layers (Retina_1
339 and Retina_2) with different time constants, with the more slowly reacting layer (Retina_2) inhibiting its
340 faster counterpart. The faster layer responds quickly to the appearance of a prolonged stimulus before it
341 is inhibited by the slow layer, forming a phasic response to stimulus onset. The mechanism ensures that
342 phasic rather than tonic responses arrive at the superficial SC from the retina.

343 The output of the Cope-Chambers model is determined by the activity in the SC_deep population. The
344 activity in SC_deep is first transformed from retinotopic co-ordinates into the Cartesian co-ordinates. The
345 centroid of the activity is then computed. The position of this centroid in the Cartesian frame determines
346 the saccadic end-point. The current model differs in that it does not compute a centroid, instead feeding the
347 SC_deep activity into the saccadic burst generator.

348 The Cope-Chambers model was parameterised by tuning the model to perform a prosaccade task in which
349 a fixed luminance point is fixated by teh model. After a fixed duration, the fixation point was extinguished
350 and a target point of fixed luminance was presented. The model was tuned so that the latency between the
351 presentation of the target and the initiation of an eye movement matched experimental data (Reulen, 1984),
352 while also matching the electrophysiological evidence of activity in a variety of brain regions. The tuning
353 of the BG model attempted to preserve as closely as possible the weights used in the original paper. Further
354 details on the parameterisation of the Cope-Chambers model are in Cope et al. (2017).

355 2.2.1 Components

356 With the exceptions of the World and FEF_add_noise populations, each neural element represents an
357 activation; the activation is governed by a first order differential equation specified in the SpineML
358 component. In the brain model, there are six different components in use: LINlinear; LINret; LINexp;
359 D1MSN and D2MSN.

360 The LINlinear component governs the activation a with a first order leaky integrator differential equation:

$$\dot{a} = \frac{1}{\tau}(a_{in} - a) \quad (3)$$

361 where τ is the time constant for the neural activation and a_{in} is the input to the neural element. a_{in} is
362 defined by an activation input and a shunting inhibition input according to:

$$a_{in} = A(1 - s_a) + \alpha R_N \quad (4)$$

363 Here, A is the activation input and s_a is the shunting inhibition state variable whose value is related to the
364 shunting input, S by

$$s_a = \begin{cases} S & S \leq 1 \\ 1 & S > 1 \end{cases} \quad (5)$$

365 R_N is a random number drawn from a standard normal distribution ($\sigma=1$, $\mu=0$) and introduces noise to the
366 activation of the neural element, with the parameter α controlling the noise amplitude.

397 The output, y , of LINlinear is related to the activation a by the piecewise linear transfer function

$$y(a) = \begin{cases} 0 & a < c \\ a - c & c \leq a \leq 1 + c \\ 1 & a > 1 + c \end{cases} \quad (6)$$

368 where c is a parameter defining the offset of the transfer function. If $c < 0$, then for zero activation ($a = 0$),
369 the output will be positive. This simulates the effect of a neural population having tonic firing. If $c > 0$
370 then the output will be zero until the activation exceeds c , simulating neurons which only fire when driven
371 by excitatory input. At this point, the naming scheme for the component becomes apparent; this is a Leaky
372 Integrator with a piecewise-linear transfer function.

373 The LINret component used for the retinal populations is similar to the LINlinear component, but with
374 no intrinsic noise and no shunting inhibitory input. It has a neural input which is identical to the activation
375 input A :

$$a_{in} = A \quad (7)$$

376 The LINexp component is a leaky integrator with an exponential transfer function. It shares the same
377 differential equation with LINlinear, but has a different input equation and a different output transfer
378 function. It has the following equation for the neural element input a_{in} :

$$a_{in} = [A + N(a - V_r^-)](1 - S) + 0.01R_N \quad (8)$$

379 where A is the activation input and N is an input which is modulated by V_r^- , a reversal potential, and
380 a , the current activation of the element. These inputs are summed and then reduced by a factor which
381 is dependent on S , the shunting input. As in LINlinear, R_N introduces normally distributed noise to the
382 element.

383 The output, y , of the LINexp component is given by

$$y(a) = \begin{cases} e^a - 0.9 & e^a \leq 1 + 0.9 \\ 1 & e^a > 1 + 0.9 \end{cases} \quad (9)$$

384 This component is used in the subthalamic nucleus (STN) population, as it gives a more physiologically
 385 accurate f-I behaviour (Wilson, 2004; Bevan and Wilson, 1999; Hallworth et al., 2003) which has been
 386 shown to allow the mapping of the basal ganglia network architecture onto an optimal decision making
 387 model (Bogacz and Gurney, 2007).

388 The D1MSN and D2MSN components are both leaky integrators, similar to LINlinear. They differ in
 389 that they have no shunting inhibition. They are used to model medium spiny neuron (MSN) populations
 390 in the striatum. As they model the fact that most MSN neurons fall into two groups; those expressing D1
 391 dopamine receptors and those expressing D2 receptors, they have a dopamine parameter that modulates the
 392 input activation, so that their equations for a_{in} are thus:

$$a_{in}^{D1} = (0.2 + d)A + 0.01R_N \quad (10)$$

393 $a_{in}^{D2} = (1 - d)A + 0.01R_N \quad (11)$

394 where d is the dopamine parameter. Varying dopamine from 0 to 1 enhances the activation in the D1 model,
 395 whereas it decreases the activation of the D2 model elements, in line with experimental observations
 396 (Harsing and Zigmond, 1997; Gonon, 1997). Note that the equation for a_{in}^{D1} differs from that used in the
 397 Cope-Chambers model, for which the cortico-striatal weights are multiplied by $(1 + d)$ rather than $(0.2 + d)$.
 398 A value of $d = 0.7$

399 The equations given above are applied to each element in a population [based on the D1MSN or D2MSN](#)
 400 [component](#). The value of the activation A (and where relevant, the shunting input, S) is determined by
 401 summing the weighted inputs to the population:

$$A = \sum_i w_i^{act} x_i^{act} \quad (12)$$

402 $S = \sum_i w_i^{sh} x_i^{sh} \quad (13)$

403 w_i^{act} and w_i^{sh} are, respectively, the weights of the i^{th} activation or shunting connections [received by the](#)
 404 [component](#); x_i^{act} and x_i^{sh} are the signals input to the activation and shunting connections.

405 2.2.2 Population activity and retinotopic mapping

406 Each population of 2500 neural elements was arranged in a 50 by 50 grid, with positions on the grid
 407 representing a retinotopic mapping similar to that found empirically both in the superior colliculus (Ottes
 408 et al., 1986) and in visual cortex (Schwartz, 1980) and assumed in this work to persist throughout the
 409 oculomotor system.

410 In a retinotopic mapping, the Cartesian co-ordinates of the light-sensitive cells in the retina, whose density
 411 varies with distance from the fovea, are transformed into the Cartesian co-ordinates of the correspondingly
 412 active cells on the colliculus. The mapping ensures that an even density of cells can be maintained in the

413 colliculus, but ensures that a group of adjoining, active, retinal neurons will always activate an adjoining
414 group of neurons on the collicular surface.

415 The mapping turns out to resemble polar co-ordinates. That is, one axis of the collicular surface specifies
416 the eccentricity of a retinal location (how far it is from the fovea) and the second axis specifies the rotational
417 angle of the retinal location; we therefore use the convention of referring to the eccentricity axis on the
418 colliculus as r and the rotation axis as ϕ .

419 The *cortical magnification factor*, $M(r)$, gives the relationship between the radial eccentricity r and the
420 retinal neural density. As in Cope et al. (2017), we use a first-order approximation of the form for $M(r)$
421 given in Rovamo and Virsu (1979):

$$M(r) = \frac{M_f}{1 + \frac{r}{E_2}} \quad (14)$$

422 The foveal magnification, M_f , is the magnification of the most central region of the retina and has a value
423 in the human of about 7.8 mm/ $^\circ$ (Rovamo and Virsu, 1979).

424 In our model, M_f is related to W_{nfs} , the width of the retinotopic neural field, W_{fov} , the width of the
425 eye's field of view and E_2 , the eccentricity at which the retinal density has halved by:

$$M_f = \frac{W_{nfs}}{E_2 \ln \left(\frac{W_{fov}}{2E_2} + 1 \right)} \quad (15)$$

426 Here, W_{nfs} is 50 (the side length of the 50x50 grid) and W_{fov} is set to 61 $^\circ$, a reduction from the
427 biophysically accurate 150 $^\circ$ due to the small number of neurons in the retinotopic neural field. E_2 is 2.5
428 (Cope et al., 2017; Slotnick et al., 2001).

429 The mapping from the retinotopic co-ordinates in the brain to rotational co-ordinates of the stimu-
430 lus/response was written down by Schwartz (1977, 1980) for measurements of striate cortex [visual
431 stimulus to electrophysiological response—Daniel and Whitteridge (1961); Talbot and Marshall (1941)]
432 and by Ottes et al. (1986) for superior colliculus data [electrophysiological SC stimulus to eye movement
433 response—Robinson (1972)]. We used the following statement of this mapping to introduce stimuli into
434 the ‘World’ input population of the brain model:

$$\phi = \frac{W_{nfs}}{2\pi} \arctan \left(\frac{\theta_y^t}{\theta_x^t} \right) \quad (16)$$

435

$$r = M_f E_2 \ln \left(\frac{1}{E_2} \sqrt{\theta_x^{t2} + \theta_y^{t2}} + 1 \right) \quad (17)$$

436 Note that we use r and ϕ as the co-ordinates on the ‘collicular surface’. Schwartz uses r and ϕ as the polar
437 coordinates of the retinal stimulus; Ottes et al. use r and ϕ as polar coordinates for the eye movement
438 response; both use u and v as the Cartesian co-ordinates of the neural map. We use θ_x^t and θ_y^t to give Euler
439 rotations for the retinal target stimulus. Note also that the form of Eqns. 16 & 17 is slightly different from
440 that given in Ottes et al. (1986) because our θ_x^t and θ_y^t are not the polar co-ordinates used in that work.

441 The mapping encompasses the entire visual field; the value of ϕ is allowed to vary from 0 $^\circ$ to 360 $^\circ$ along
442 its axis. Effectively, the two contralateral colliculi found in the biology are incorporated into a single,

443 square map, avoiding the need to carry out the kind of ‘colliculus gluing’ described in Tabareau et al.
 444 (2007).

445 It is straightforward to show that the reverse mapping is given by:

$$\theta_x = E_2 \left(e^{\frac{r}{M_f E_2}} - 1 \right) \cdot \cos \left(\frac{2\pi\phi}{W_{nfs}} \right) \quad (18)$$

446

$$\theta_y = E_2 \left(e^{\frac{r}{M_f E_2}} - 1 \right) \cdot \sin \left(\frac{2\pi\phi}{W_{nfs}} \right) \quad (19)$$

447 where we have dropped the t superscript on θ_x & θ_y , as these equations transform a collicular location into
 448 rotations of the eye.

449 Fig. 3 shows the result of the mapping for a view of two cross-shaped luminances. One cross illuminates
 450 the fovea, which results in a large comb-shape of activity. The more peripheral cross produces (in FEF) an
 451 indistinct object centred at a larger value of r .

452 2.2.3 Network

453 Briefly, the model consists of input from the World population (see Fig. 2, green population box)
 454 producing activity in an ‘express’ pathway to superior colliculus (purple) and simultaneously in cortex,
 455 represented here by the FEF population (grey boxes in Fig. 2). The express pathway causes short latency
 456 activity in the superficial superior colliculus, which directly innervates the deeper layers of the superior
 457 colliculus (SC_deep). Activity in FEF generates firing in a thalamo-cortico-basal ganglia loop. The output
 458 of the basal ganglia is the substantia nigra pars reticulata (SNr) which tonically inhibits SC_deep. If a
 459 location of activity in FEF is able to dominate selection in the basal ganglia circuit, the corresponding
 460 location in SNr will dis-inhibit and activity will build up in SC_deep encoding the saccade end point.

461 Connections shown in red are one to one connections; dark blue projections indicate a connectivity pattern
 462 which ‘fans out’ with a 2-D Gaussian kernel; lighter blue connections from the subthalamic nucleus (STN)
 463 to SNr and globus pallidus externum (GPe) are diffuse, all-to-all connections and projections coloured
 464 green are one-to-one connections that decay towards the fovea so that foveal activity in FEF does not
 465 swamp the basal ganglia which would prevent peripheral luminances from ever being selected. Note
 466 that SC_deep contains two recurrent connections; one is excitatory, with a Gaussian kernel mapping and
 467 the other implements tecto-tectal inhibition, which increases the inhibition between activity in opposite
 468 hemispheres of the field of view (Gian G. Mascetti and Jorge R. Arriagada, 1981; Olivier et al., 2000)
 469 helping to resolve competition between saccades to the left and right. The tecto-tectal inhibitory connection
 470 is *not* present in the Cope-Chambers model. In all other respects the model is as described in Cope et al.
 471 (2017). We have not listed the parameters of the network in tabular form here, instead, the reader is referred
 472 to the SpineML declarative specification of the model from the link given in SUPPLEMENTAL DATA.
 473 The easiest way to access this information is by using SpineCreator.

474 2.3 Brainstem model

475 We implemented a saccadic burst generator (SBG) based on the connectivity outlined in Gancarz and
 476 Grossberg (1998). The SBG network for two of the model’s six channels is shown in Fig. 4. In the brainstem
 477 model, we use the word ‘channel’ to mean a set of populations of neurons which are involved in actuating
 478 a single extraocular muscle. SBG channels are arranged in pairs, actuating opposing muscles. There is
 479 one pair of channels which actuates the superior and inferior rectus muscles, causing vertical rotations

480 of the eye in a roughly parasagittal plane (the eye moves up or down). Another pair actuates the lateral
 481 and medial rectus muscles, causing horizontal rotations of the eye. The third pair actuates the superior
 482 and inferior oblique muscles which contribute to vertical as well as oblique rotations. Activity from the
 483 output layer of superior colliculus (SC_avg) is fed into each channel, which sums the activity it receives and
 484 processes it in populations each of a single neural element representing all the neurons in that population.
 485 Each channel of the SBG functions to create the motor neuron activations that are required to accelerate
 486 the eye in a particular direction, then hold the eye in its new position against the returning force generated
 487 by the elastic properties of the muscles. The required motor neuron activations are therefore a combination
 488 of features: a brief burst of increased activity that accelerates the eye; followed by a period of activity that
 489 is less than the burst firing rate but higher than the tonic rate that exists when the eye is at the centre. This
 490 holds the eye in its new position.

491 The SBG connectivity produces each of these features separately, then sums them to create the desired
 492 ‘bump and tonic’ activation time series. The input to the first population in the SBG, the long-lead burst
 493 neurons (LLBNs), is conceived as originating from one of the deep layers of the superior colliculus. The
 494 activity of the LLBNs are passed to excitatory burst neurons (EBNs) which, in turn, inhibit the LLBNs via
 495 the activity of the inhibitory burst neurons (IBNs). This feedback loop has a transmission delay, which
 496 allows activity to build up in the EBNs before the inhibition is activated and the activity is then reduced
 497 again. This mechanism generates the ‘bump’.

498 The generation of the ‘tonic’ phase of the required time series is achieved simply by integrating the bump
 499 over time and multiplying by a some small gain factor. This is the function of the tonic neurons (TNs).
 500 The firing rate of the motor neuron defines the amount of force applied to the eye by that muscle. Thus,
 501 the integral of the ‘bump’ defines how far the eye moves in that channel’s direction. The gain and delay
 502 parameters in the LLBN-EBN-IBN-LLBN feedback loop therefore have to be tuned such that the endpoint
 503 of the saccade is reasonably accurate. Furthermore the restoring force generated by the elasticity of the
 504 muscles is dependent on the radial distance. The value of the new tonic firing rate, after the ‘bump’ is
 505 dependent on the end location of the eye. If the ratio between the EBN firing rate and the TN firing rate is
 506 not exactly correct, the eye will drift away from the saccade endpoint after the saccade has been completed.
 507 The EBN-TN connection strength is therefore tuned such that the TN firing rate yields a stable eye position
 508 across a range of eye eccentricities.

509 The omnipause neurons (OPNs) are tonically active and inhibit the EBNs. The activity of the OPNs is
 510 itself inhibited by activity in the LLBNs. The purpose of this arrangement is to ensure the eye does not
 511 move in response to neural noise.

512 Each mean activity of all the neurons in each SBG population (except the TNs) is defined by a single
 513 leaky integrator, first order differential equation.

$$\frac{da}{dt} = \frac{1}{\tau}(y - a) \quad (20)$$

514 where a is the activation of the nucleus, and τ is the time constant of the nucleus. y is a piecewise linear
 515 function of the weighted sum of inputs to the nucleus and is given by

$$y(IN) = \begin{cases} 0 & IN \leq b \\ IN - b & b \leq IN \leq 1 + b \\ 1 & IN \geq 1 + b \end{cases} \quad (21)$$

516 where b is the IN axis offset. IN is the weighted sum of inputs to the nucleus and is given by,

$$IN = \sum_m^M w_{mn} a_m \quad (22)$$

517 where a_m is the activation of the m^{th} afferent nucleus. w_{mn} is the connection strength between the m^{th}
518 afferent nucleus and the current nucleus. The activity of the TNs are defined as

$$\frac{da}{dt} = \frac{1}{\tau} y \quad (23)$$

519 with an identical piecewise linear transfer function as the other SBG populations.

520 2.4 Biomechanical eye

521 The output signals of the brainstem's motoneuron (MN) populations are used to drive the biomechanical
522 model. The MN output signal in each brainstem channel is normalised in the range [0 1] and represents the
523 mean firing rate of the neurons that innervate the extraocular muscle for that channel. The biomechanics
524 are used not only to get tangible feedback on the simulated saccades including motion trajectories, but
525 to add one more modelling dimension related to the inertial properties of the eye plant including muscle
526 properties.

527 The biomechanical eye model, implemented using the OpenSim framework (Seth et al., 2011), is
528 anatomically represented by a sphere of uniform mass distribution. The diameter of the eye is 24 mm for
529 adults, with small variations between individuals; the mass of the eye is 7.5 grams. The eyeball is actuated
530 by six extraocular muscles (EOMs). The EOMs are arranged in three pairs forming a cone inside the orbit
531 with the apex being located inside the cranium in a tendonous ring called the annulus of Zinn. An important
532 feature of the oculomotor system which greatly affects its overall behavior is the existence of dynamic
533 EOM pulleys. Their role is to guide the pivot point of the EOMs. In our model, a pulley for each EOM has
534 been modeled by a point on the orbit whose location depends on the current eye orientation.

535 An illustration of the biomechanical eye model is given in Figure 5, while Figure 5 depicts the head
536 model used in the proposed framework.

537 Two types of muscle models of different complexity are supported. The first models muscles using linear
538 path actuators. This simplistic model of ideal muscles can be easily integrated with high level brain models.
539 As described above the muscles are wrapped around the eye. The more complex model supported is based
540 on the Thelen model (Thelen, 2003) that is also supported by OpenSim and implements Hill-type muscles.
541 It includes realistic muscle wrapping geometric entities of the muscle fibers, while it accommodates for
542 both activation and contraction dynamics. The dynamics of muscular forces can be split into: 1) The
543 elasticity of the muscles. 2) A delay between the onset of the afferent excitatory signal and the actual
544 muscle contraction, caused by the transmission time of the action potentials and by the necessary calcium
545 release at the muscle fibres.

546 The force applied by EOMs is controlled by an excitatory signal supplied by motoneurons in the brainstem.
547 The neural drive to produce a saccadic eye movement can be characterized by a pulse component to
548 overcome the viscoelasticity of the orbital plant, a step component to stabilize the eye in the new position,
549 and a slide component that models the gradual transition between the pulse and step.

550 Passive forces due to the fatty tissues inside the eye orbit also affect eye dynamics. Their role is critical in
551 eliminating the influence of head and body movements. We incorporated a custom torque, t , which acts
552 like a rotational spring-damper apparatus, resisting eyeball movements. It has elastic and viscous properties
553 governed by $t = -KR - CU$ where R is the eye's orientation and U is its angular velocity. K and C are
554 constants. A fuller description of the biomechanical model can be found in Papapavlou and Moustakas
555 (2014).

556 2.5 Model development framework

557 The Cope-Chambers model was originally developed to run on the BRAHMS model execution framework
558 (Mitchinson et al., 2010; Mitchinson and James, 2015). To run a BRAHMS model, the researcher must
559 develop *BRAHMS components* for the various neural elements. A BRAHMS component is a program-
560 matically coded implementation of the behaviour of the component. It may have an arbitrary number of
561 inputs and outputs and may be written in C, C++, Python or MATLAB. The Cope-Chambers model's
562 components were hand written in C++ and MATLAB. A BRAHMS *SystemML* file describes how the
563 different components connect together and how data is passed between them (Mitchinson et al., 2010). The
564 main BRAHMS program first reads the SystemML file, then dynamically loads all the required components
565 before executing the system.

566 In the current work, the Cope-Chambers model was reproduced using the declarative SpineML markup
567 language (Alex Cope and Paul Richmond, 2014; Richmond et al., 2014), with the help of the graphical
568 SpineML model editing software called SpineCreator (Cope et al., 2015, 2016). SpineML, which is a
569 development of the NineML specification (INCF Task Force on Multi-Scale Modeling, 2011), describes
570 neural populations and their projections in a highly structured format in which neuron bodies, pre- and post-
571 synapses are described in terms of *SpineML components*. These are similar to the components provided by
572 BRAHMS, but in this case, the components are an XML description of the functionality of the component,
573 rather than a programmatic implementation, with one XML file per component. A SpineML *network layer*
574 file then describes which components are used in the model, and how they are connected together. Finally,
575 a number of SpineML *experiment layer* files specify how the model described in the network layer can be
576 executed. In the experiment layer, the execution duration and timestep can be specified, along with input
577 conditions, connection lesions and component parameter updates. A description of SpineML is given in
578 Richmond et al. (2014); the definitive definition is found in the schemas (Cope et al., 2014). SpineCreator,
579 in its rôle as a graphical editor for the SpineML format, was used to generate the SpineML files describing
580 the model. It was also used to generate the diagrams of the model.

581 As a declarative format for model specification, SpineML is agnostic about how the model is executed. A
582 number of simulation engines can be utilised, including DAMSON (Richmond, 2015), GeNN (Nowotny,
583 2011; Nowotny et al., 2014) and BRAHMS (used here). The simulation engine incorporating BRAHMS is
584 called SpineML_2_BRAHMS (Cope and James, 2015). SpineML_2_BRAHMS is a collection of XSLT
585 stylesheets which first generate and compile C++ BRAHMS components from the SpineML component
586 layer description files. SpineML_2_BRAHMS then uses the SpineML network and experiment layer files
587 to generate a BRAHMS SystemML description of the model. Finally, SpineML_2_BRAHMS executes the
588 model, now described entirely as a BRAHMS system, via a call to the BRAHMS binary. A number of
589 additional hand-written components are present in SpineML_2_BRAHMS providing the inputs (constant
590 inputs, time-varying inputs, etc) which the modeller specifies in the experiment layer.

591 In addition to the brain model components, all of which are code-generated using SpineML_2_BRAHMS as
592 described above, two hand-written components are integrated into the model: The biomechanical eye model

593 and a sensory input component. The sensory input component takes the eye's rotational state and the state
 594 of the experimental luminances and projects a retinotopic activity map into the brain model. Both of these
 595 BRAHMS components were hand-written in C++. To incorporate these components into the SpineML
 596 model, a SpineML_2_BRAHMS *external.xsl* file was used. The external.xsl file scheme for incorporating
 597 external BRAHMS components into a SpineML model was a new SpineML_2_BRAHMS feature motivated
 598 by the current work. Fig. 6 shows the workflow, in which the model specification files (blue box - a
 599 combination of SpineML files and C++ code), are processed (green box) into a BRAHMS system (red
 600 box).

601 Finally, numerical integration of the biomechanical eye model is based on the Kutta-Merson integration
 602 method.

603 2.6 Integrating the models and closing the loop

604 The Cope-Chambers model closed its loop by passing the centroid of activity in SC_deep (once it had
 605 surpassed a threshold) back to the code that controlled the world, which would then use this location to
 606 instantaneously change the model's view of the world. In our extended model, it was necessary to connect
 607 the output of the brain model back to its input via the saccadic burst generator model and the biomechanical
 608 eye. The resulting state of the eye, rather than the centroid of the superior colliculus, was used to compute
 609 the input to the brain, given the luminances visible in the world.

610 Thus, the information flow in the model is as follows: Luminances in the world have their locations
 611 computed in the eye's frame of reference, based on the rotational state of the eye. The locations of the
 612 luminances on the retina are transformed into a retinotopic co-ordinate system which determines the
 613 activity in the 'World' population (named to mean the 'world as the eye sees it', rather than the world
 614 frame of reference) which is the input for the brain model. The target luminance for a saccade is selected,
 615 as described earlier, via cortical and sub-cortical loops through the basal ganglia model and activity for
 616 the winning end-point builds up in the deep layer of superior colliculus. This activity excites activity
 617 in the correct proportions within the 6 channels of the saccadic burst generator whose output state, the
 618 motoneurons send a rate-code signal (normalised between 0 and 1) into the biomechanical eye model. The
 619 rotational state of the eye model is fed back to participate in the computation of the retinotopic luminance
 620 activity in 'World', completing the loop.

621 A number of studies have considered the form of the connection between the deeper layers of the superior
 622 colliculus and the saccadic burst generator (Van Gisbergen et al., 1985; Ottes et al., 1986; Waitzman et al.,
 623 1991; Groh, 2001; Arai et al., 1994; Goossens, 2006; Tabareau et al., 2007; van Opstal and Goossens, 2008;
 624 Goossens and van Opstal, 2012), which has become known as the spatial temporal transform (STT). The
 625 spatial aspect of the transform is thought to be implemented by a weight-mapping (Tabareau et al., 2007;
 626 Arai et al., 1994) and we follow this idea. Arai and co-workers trained a 20x20 neural network model
 627 of the superior colliculus to discover the weight map under the assumption of 2D Gaussian activation
 628 profiles (Arai et al., 1994)—that is, they assumed that the activity in superior colliculus for any saccade was
 629 a size-invariant 2D Gaussian hill of activity. The training approach of Arai et al. (1994) was not feasible in
 630 this study due to the length of time required to run our model and its stochasticity, which meant multiple
 631 runs of the model were necessary in order to generate output statistics. Tabareau et al. (2007) wrote down
 632 a theoretical form of the weight map, obtained by inverting the mapping of Ottes et al. (1986) and the
 633 assumption of invariant 2D Gaussian activity profiles in SC, which is equivalent to:

$$w(r, \phi) = i e^{jr} \sin(l\phi + k) \quad (24)$$

634 where r and ϕ are co-ordinates on the collicular map and i, j, k and l are parameters of the function
 635 (compare with Eq. 3 of Tabareau et al. (2007)). As they found it closely resembles the results of Arai et al.
 636 (1994), and it is a simple formulation, we considered it as the means to generate the six weight maps in our
 637 own model. One barrier to the use of this weight map was the Cope-Chambers model's violation of the
 638 *invariant integral hypothesis*. This states that the number of spikes emitted by a neural element during a
 639 saccade (or in our model, the integral of the neuron's output during the saccade) should be a function only
 640 of its position within the hill of collicular activity. That is, for any time-dependent hill of activity $A(z, t)$ at
 641 $z = (r, \phi)$ on the collicular surface, the integrated activity A_x in an element at a vector x away from z is

$$A_x = \int_t A(z - x, t) dt \quad (25)$$

642 which is invariant for all z . **This requirement is fulfilled by spatially invariant 2D Gaussian profiles, whose**
 643 **time-course (how quickly they grow and then diminish) is always the same.**

644 However, the very mapping on which the Tabareau et al. (2007) result is based leads to a very *variant*
 645 activity profile **in the SC_deep layer** of the Cope-Chambers model. A luminance of a given size which
 646 excites activity near to the fovea causes activity in a large number of neurons in each retinotopic layer,
 647 whereas activity far from the fovea excites a much smaller region. This effect is clearly demonstrated in
 648 Fig. 3 for equal sized targets both on and distal from the fovea.

649 To understand the need for this invariance, consider the effect of a 2D Gaussian hill in SC_deep which
 650 elicits a successful horizontal saccade of 10° . Activity from the 2D Gaussian, passing through the weight
 651 maps will excite the superior and inferior rectus channels by an equal, balanced amount, so these cancel out,
 652 allowing the eye movement to be horizontal. The amount of activation passed to the lateral rectus muscle
 653 results from a convolution of the Gaussian and the exponential component of the weight map relationship
 654 in Eq. 24. If the Gaussian hill now appears further along the collicular surface, coding for a 20° saccade,
 655 *and also becomes smaller*, we can still argue that the vertical component signals to superior/inferior rectus
 656 muscles will cancel out, and we could imagine that the exponential component of Eq. 24 is correctly
 657 parameterised to compensate for the smaller hill. However. Now consider a 2-D Gaussian hill which codes
 658 for a 10° saccade which is 'up, and to the right' in equal proportions. That means that the hill will sit on
 659 the boundary between the weight maps for the 'up', and the 'right' muscles. Now, if the hill moves to
 660 the $r = 20^\circ$ location on the colliculus, *and also reduces in size*, it will excite only the periphery of the
 661 sine; the exponential increase of the map along r is not guaranteed to compensate for the reduction in the
 662 convolution of the Gaussian hill and the sinusoidal component of the weight map.

663 This led us to hypothesise that the retinotopic mapping **to the SBG** be preceded by an associated widening
 664 projection field such that the hill of activity in a '**final**' deep layer of superior colliculus is **invariant with**
 665 **position on the map**. There are a number of locations in the system in which this widening projection
 666 field could exist. It could be implemented in the projections between the retinal populations and the
 667 superficial layer of SC along with the projection between the World and the FEF population. However,
 668 this would affect activity within the basal ganglia of the model, contradicting a result in Cope et al. (2017)
 669 which explains the 'hockey stick' profile for saccade latency as a function of saccade eccentricity. Instead,
 670 we suggest that a widening projection field is encoded within the superior colliculus itself, a complex,
 671 multi-layered structure which could quite plausibly support such a function. Indeed, such widening activity
 672 can be seen in the stimulation experiments in Vokoun et al. (2010) and Vokoun et al. (2014). In Ghitani
 673 et al. (2014), from the same research group, evidence is presented for an excitatory and widely projecting
 674 pathway from the stratum griseum intermediale (equivalent to our SC_deep) to the more superficial layers

stratum opticum and stratum griseum superficiale. Although this pathway is a ‘wide’ projecting field, the experiments do not indicate whether the projection *widens* along the rostral-caudal axis of the SC. Bayguinov et al. (2015) presents evidence for another projecting field within SC whose connectivity pattern *does* change along the rostral-caudal axis. This projection is inhibitory in nature. Although neither of these results precisely match the widening, excitatory projection field hypothesised here, they do indicate that such connection patterns are plausible. Although in this work we do not model the SC in detail, we extended the model with a third functional layer named SC_deep2, shown in Fig. 7(b) (Cope-Chambers has only the two layers SC_sup and SC_deep). We introduced a widening projection based on a Gaussian projection field whose width, $\sigma(r)$ varies in inverse proportion to the magnification factor, $M(r)$, given in Eq. 14 according to:

$$\sigma(r) = \frac{m_\sigma}{M(r)} - \frac{m_\sigma}{M^0} + \sigma_0 \quad r > r_0 \quad (26)$$

m_σ is a scalar parameter which determines the ‘magnitude of the widening’. M^0 is the ‘starting’ magnification factor; within the foveal region ($0 \leq r \leq r_0$), the projection field is not allowed to widen and so

$$\sigma(r) = \sigma_0 \quad r \leq r_0 \quad (27)$$

which makes σ_0 the width of the Gaussian projection field within the foveal region. (Note that the value chosen for the width of the foveal region, r_0 is not identical to the foveal shift parameter used in the *DecayingAtFovea* projections into striatum.) The *Widening Gaussian* projection weight, $w(r, d)$ is then computed as:

$$w(r, d) = e^{-\frac{d^2}{2\sigma(r)^2}} \quad (28)$$

where d is the distance between the source and destination elements in the collicular plane. m_σ was set to 50, σ_0 was 0.3, M^0 was 12.43 and r_0 was 20.

A further issue regarding the use of the theoretical weight map in Tabareau et al. (2007) was that it does not consider the existence of the oblique extraocular muscles. There is evidence that only two dimensional information is encoded in superior colliculus (Wurtz and Goldberg, 1972; Hepp et al., 1993; Van Opstal et al., 1991), but the eye is actuated by six extraocular muscles. In order to find out a possible form for the input to the oblique muscles we carried out a training process which depended on a centroid computation in SC_deep. For the four rectus muscles, the resulting weight maps resembled those found by Arai et al. (1994). The trained maps for the oblique muscles had a form very close to those for the inferior and superior rectus channels, but with a smaller magnitude. The inferior oblique map resembled the superior rectus map and the superior oblique map resembled the inferior rectus. When parameterising the theoretical weight maps, we set the inferior/superior oblique maps to be 1/10th of the superior/inferior rectus maps, respectively. Interestingly, this suggests that there is a built-in synergy between the vertical and oblique channels in the eye, although the results will show there is some systematic change in the oblique error with saccade end-point location.

Tabareau et al. (2007) give a formulation for the weight maps in which it is possible to project both a positive and a negative weight. In our model, all projections from SC_deep are excitatory. This means that each channel has a weight which follows the form:

$$w(r, \phi) = i e^{jr} \sin \left(\frac{2\pi\phi}{W_{nfs}} + k \right) \quad (29)$$

710 where i , j and k are per-channel parameters for the weight maps. k is determined by the mapping. Only the
711 positive part of the sine is utilised. i and j are parameters to be found.

712 The saccadic burst generator model was originally conceived with the assumption of a step input, which
713 returns to zero activity at a suitable time to curtail the saccade and avoid staircase saccades (Gancarz and
714 Grossberg, 1998). In our model there is no such mechanism to reduce activity in SC_deep, and elsewhere.
715 Although a successful, accurate saccade towards a target luminance will remove the excitation which caused
716 the activity in SC_deep by bringing the target luminance within the masked, foveal region, the activity
717 in SC decays too slowly to avoid additional saccadic movements. We found it necessary to hypothesise
718 an inhibitory feedback mechanism from the SBG to the brain model. This is shown in Fig. 4, which
719 indicates how the output from the inhibitory burst neurons (IBN) of the SBG model are used to feed back
720 an inhibitory signal to the SC_deep, thalamus and FEF populations in the brain model, resetting them ready
721 for the next saccade. **There is evidence for inhibitory projections to SC from the propositus hypoglossi**
722 **nucleus (Corvisier and Hardy, 1991), which lies within the brainstem, upstream from motoneurons, and**
723 **has been shown to encode eye velocity (Dale and Cullen, 2013).**

724 The output signals from the six channels of the SBG were connected to the six motoneuron inputs of the
725 biomechanical eye. The signal was normalised; a value of 1 meaning that all the motoneurons in the output
726 population were firing at their maximum rate and the force exerted by the relevant extraocular muscle
727 was maximal. Channels innervated extraocular muscles as follows: Up: superior rectus; Down: inferior
728 rectus; Right: medial rectus; Left: lateral rectus; Z+: superior oblique; Z-: inferior oblique. Because the
729 medial rectus induces a rightward rotation of the eye, our single virtual eye is a *left* eye. The OpenSim
730 implementation of the biomechanical eye was ‘wrapped’ (in the software sense) in a BRAHMS component.
731 This made it possible to integrate the OpenSim model into the BRAHMS framework. The wrapper ensured
732 that the input and output signals were correctly transferred and, importantly, handled the disparity in the
733 solver timesteps used in the OpenSim model (25 ms) and the neural model (1 ms). This was achieved by
734 having the BRAHMS wrapper create a separate thread to run the OpenSim model. The BRAHMS wrapper
735 component was called on each 1 ms timestep, receiving the instantaneous activations from the motoneurons
736 in the SBG. These activations, and the current simulation time, were written into a shared memory area,
737 accessible by the OpenSim thread. Running independently, the OpenSim thread would update its inputs
738 (using the most recent values in the shared memory area) whenever the simulation time had increased
739 by 25 ms. It would then recompute its outputs (the rotational state of the eye) and write these into the
740 same shared memory. The BRAHMS wrapper would update its outputs whenever they were changed in
741 the shared memory by the OpenSim thread. A direct connection of the six outputs of the BRAHMS eye
742 model component to the six inputs of the worldDataMaker BRAHMS component was specified in the
743 SpineML_2_BRAHMS external.xsl file.

744 The eye model outputs its rotational state at each timestep. The rotational state is used to compute
745 the view of the world in the eye’s frame of reference. To simplify the calculation, the luminances exist
746 on a spherical surface at the centre of which is the eye. A hand-coded BRAHMS component called
747 worldDataMaker computes the projection of the luminances into the eye’s frame of reference and then
748 converts this representation into a retinotopic map to pass into the brain model. The input to the brain
749 model is thus able to change continuously, on every timestep, rather than in a step-wise fashion when a
750 saccade occurs, as in the Cope-Chambers model.

751 In the worldDataMaker BRAHMS component, the rotational state of the eye was used to construct
752 Euler rotation matrices which transformed between the world’s frame of reference and the eye’s frame of
753 reference. The worldDataMaker component received a specification of the world luminances in a JSON

754 file called luminances.json at the start of each simulation. luminances.json specified the position, shape,
755 size, luminance, appearance time and disappearance time of an arbitrary number of luminances. With this
756 information, the instantaneous rotational state of the eye and the parameters of the retinotopic transform, it
757 was able to compute the instantaneous input to the brain model.

758 The final models, on which the results of this paper are based are named ‘TModel3’, ‘TModel4’ and
759 ‘TModel5’. Descriptions of these, and earlier versions of the model can be found in the code repository
760 given in SUPPLEMENTAL DATA.

3 RESULTS

761 3.1 Weight maps

762 We found the best parameters for the exponential in Eq. 29 (i and j) by a manual tuning process. After
763 selecting values for i and j in either the horizontal or vertical/oblique channels, we ran the model 6 times
764 at each of 8 target eccentricities (7° – 14°) which were purely in the direction of the newly parameterised
765 channel. The training saccades were produced as described below in Sect. 3.3, with the same fixation
766 and target luminances (crosses of magnitude 0.2 and 0.3) but with the fixation offset and target onset
767 occurring at 0.2 s. We measured the end-point of the saccade by detecting the location at which the saccade
768 velocity had dropped below 0.005 of its peak. We iterated until the mean saccade endpoint plotted versus
769 target was close to the ideal straight line—see Fig. 8(a) & (b). We applied the same parameters to both
770 directions of each channel; $i_{up} = i_{down} = 0.00195$, $j_{up} = j_{down} = 0.075$, $i_{left} = i_{right} = 0.0016$ and
771 $j_{left} = j_{right} = 0.067$.

772 The resulting weight maps (where the oblique maps are $1/10^{\text{th}}$ of the vertical maps, as described earlier)
773 are shown in Fig. 9. First, recall that the r axis of the neural surface corresponds to the amplitude of a
774 saccade and the ϕ axis indicates the polar direction of the saccade, as described in Sect. 2.2.2 and Fig. 3.
775 Fig. 9(a) shows the weight map for the muscle which rotates the eye to the left. As we modelled a left
776 eye, this actuates the lateral rectus muscle. The exponential rise of Eq. 29 is seen in the r direction; as r
777 increases, so the connection strength to the SBG channel rises exponentially. The connection strength is
778 greatest along the centre line, for a value of ϕ which corresponds to a purely leftward movement. Note that
779 ϕ is presented in neural coordinates, and not in degrees or radians; $1 \leq \phi \leq 50$ corresponds to a range of
780 0° to 360° ; $\phi = 38.5$ corresponds to movements left. The connections strength drops away sinusoidally
781 as ϕ moves away from the centre line at $\phi = 38.5$. In regions of the map for which there is no leftward
782 movement, that is, in the half of the map which corresponds to any movement with a rightward component,
783 the ‘left’ weight map is 0. Fig. 9(d) shows the weight map for rightward movements, actuating the medial
784 rectus muscle of the eye. The line of maximum connection strength is along $\phi = 13.5$. The map is a mirror
785 of Fig. 9(a), reflected about the line $\phi = 26$. The ‘left’ and ‘right’ weight maps are orthogonal; the non-zero
786 region of the ‘left’ map is zero in the ‘right’ map and vice versa. Fig 9(b) & (d) show the weight maps
787 for downward and upward eye movements; the ‘down’ map activates the SBG channel for the inferior
788 rectus muscle, the ‘up’ map activates the superior rectus. Note that ‘down’ is not orthogonal either to ‘left’
789 or ‘right’ because a saccade down and left is achieved by simultaneously activating both the lateral and
790 inferior rectus muscles. However, the ‘up’ map is orthogonal to the ‘down’ map and spans the edges of
791 the surface where ϕ rolls over from 1 to 50. The line of maximum connection strength for the ‘up’ map is
792 along $\phi = 1$; for ‘down’ $\phi = 26$. Based on the training described in Sect. 2.6, the maps driving the superior
793 oblique (‘Z+’) and inferior oblique (‘Z-’) muscles were set to $1/10^{\text{th}}$ of the ‘down’ and ‘up’ maps.

794 3.2 Saccade accuracy

795 In Fig. 8, we showed the result of running the model to targets located on the principle axes, on which
796 the model was trained. We then simulated single saccades to targets in one hemifield of the eye's field of
797 view, with eccentricities between 6° and 14.5° . As in the training, we ran the simulation 6 times for each
798 target, $\theta^t = (\theta_x^t, \theta_y^t, 0)$ to obtain mean saccade end-points. Fig. 10 shows saccade accuracy results for an
799 entire hemifield in the naïve model which passed the output of SC_deep directly to SBG via the weight
800 maps. The ratio of the magnitude of the error vector to the magnitude of the target vector is plotted using a
801 colour map. This ratio is shown for the full, three dimensional error vector in Fig. 10(a) and for the x , y
802 and z components in Figs. 10(b)–(c). Inspection of Fig. 10(a) shows that the end-point error is minimal
803 along the principle axes ($\theta_x^t = 0$ or $\theta_y^t = 0$) and maximal near the 45° oblique targets (blue lines) with the
804 end point error as high as 80% of the programmed saccade magnitude. The x component error map in
805 Fig. 10(b) shows the same trend, mirrored about the 'Target X' axis, whereas the y and z component errors
806 are, relatively, much smaller. Because the x component of the error is clearly contributing to end point
807 errors which would not be considered 'on target', especially for oblique saccades, we considered the effect
808 of the non-uniform size of the hill of activity in SC_deep.

809 In our model, the location, *size* and shape of activity in FEF, the basal ganglia, thalamus and superior
810 colliculus is eccentricity dependent, in line with the retinotopic mapping stated by Ottes et al. (1986). More
811 eccentric targets generate reduced activity, because fewer retinal neurons are excited far from the fovea.
812 Cope et al. (2017) showed that this relationship can explain increased saccadic latencies for distal targets,
813 resulting from reduced activity in the decision making circuitry of the basal ganglia. However, the notion
814 that activity in superior colliculus is eccentricity-dependent conflicts with the result of Tabareau et al. (2007),
815 who showed that an invariant hill of activity was required if this complex logarithmic weight mapping was
816 to be used to drive a two-degree-of-freedom saccadic burst generator, and also with experimental findings,
817 which do not show significant eccentricity dependence, at least in the burst layer (Anderson et al., 1998).

818 To bring our model in line with these results, whilst maintaining the eccentricity dependent activity in
819 basal ganglia, we hypothesised that a 'widening projection' exists between two maps in superior colliculus.
820 As described in Sect. 2.6, there is now experimental evidence for similar projections (Ghitani et al., 2014;
821 Bayguinov et al., 2015) making this a plausible suggestion. Activities in one SC_deep layer remains
822 eccentricity-dependent, with loops back to thalamus and cortex and through basal ganglia. This activity
823 is then fed through a projection, which applies a Gaussian projection field, whose width increases with
824 increasing stimulus eccentricity according to Eq. 28. The activity in this second SC_deep layer is then
825 fed to the weight maps of the SBG. This model was called 'TModel4'. TModel4 was parameterised such
826 that its horizontal and vertical error was similar—so that its equivalent of Fig. 8 showed a similar sum of
827 squares error.

828 Figs. 11(a)–(d) show the percentage errors for TModel4. First of all, note that the error magnitudes
829 are much smaller. The mean errors are smaller for every axis. The largest errors produced by the model
830 are approximately 15%, which are within the boundaries of what some authors have suggested would be
831 regarded as an accurate saccade (McPeek and Keller, 2002; McPeek, 2006). The magnitude of the largest
832 error vector is approximately 1.5° .

833 This result indicates that the exponential part of the Ottes et al. weight map from SC to the SBG cannot on
834 its own compensate for the eccentricity-dependent size of the hill of activity. The introduction of a widening
835 projection field substantially improves the mean accuracy of saccades across the field of view. We therefore
836 suggest that the transformation between retinotopically mapped activity, and eccentricity-independent

837 activity width occurs within the superior colliculus and works alongside a simple, monotonically increasing
838 weight map between SC and the SBG channels.

839 3.3 Single saccades

840 Having finalised the model by setting the weight maps, we then proceeded to exercise the model
841 (TModel4), starting with saccades to a single target; prosaccades. Fig. 12(a) shows 9 representative
842 saccades to a single target luminance. Initially, the eye had rotational state $\theta_x = \theta_y = \theta_z = 0$ with
843 its fovea directed at a fixation luminance cross (span 6°, bar width 2°) of magnitude 0.2 (in arbitrary
844 units). At a simulation time of 0.4 s, the fixation luminance was set to 0 and a target luminance cross
845 of the same dimensions as the fixation but with magnitude 0.3 was illuminated at one of the 9 different
846 locations, marked by crosses in Fig. 12(a). The resulting trajectories are plotted, with colour indicating the
847 relationship between trajectories and target crosses. The approximate end-point error is visible in this figure,
848 although the last point in each trajectory is the saccade position at 0.8 s and not the velocity-based end-point
849 described above. Figs. 12(b) and (c) show the rotational components of the blue and red trajectories in
850 Fig. 12(a) along with the target and fixation luminance values. Rotations are the eye's Euler rotational
851 components in the world frame of reference.

852 3.4 Saccade Latencies

853 To verify that our implementation of the brain model has the same functionality as that reported in Cope
854 et al. (2017), we investigated the effect on saccadic response times of: target eccentricity; and any gap
855 or overlap between fixation off-time and target on-time. We showed that the full model reproduces the
856 'hockey stick' shape shown in Fig. 7 of Cope et al. (2017) for horizontal [Fig. 13(a)], vertical [Fig. 13(b)]
857 and oblique saccades (not shown). The latency increases with eccentricity far from the fovea because the
858 retinotopic mapping reduces the activity in the basal ganglia for more eccentric targets (see Fig. 3). Closer
859 to the fovea, the **effect of the foveal mask on** the activity in FEF again leads to reduced input into the basal
860 ganglia and an increased time to achieve disinhibition in SNr.

861 Fig. 13(c) shows latencies achieved when varying the time between fixation offset and target onset. This
862 is termed the *gap condition*; and is represented by a scalar value which, if positive, refers to a gap between
863 fixation offset and target onset, and when negative, signifies an overlap, with the fixation luminance
864 persisting past the time at which the target is illuminated. A negative gap is also termed an *overlap*. Again,
865 we verify the behaviour presented in Cope et al. (2017), explained as resulting from the inhibition of
866 the cortico-thalamic loop by SNr. In the gap condition, when the fixation luminance is removed, activity
867 in STN immediately begins to decay, allowing SNr activity to reduce and thereby reducing inhibition
868 on thalamus, allowing the target luminance to build up quickly in FEF, thalamus and through the basal
869 ganglia's striatum and SNr. The shape of the curves in Fig. 13(c) matches the results in Cope et al. (2017)
870 for target luminances of 1 and 0.6; for overlaps longer than 100 ms (gap < -100 ms), the latency becomes
871 constant; the saccade is programmed whilst the fixation is present, with the target luminance inducing
872 sufficient activity in striatum to 'break through' the SNr inhibition caused by the fixation. If the target
873 luminance is reduced to 0.3, the balance is altered in favour of the fixation and the latency vs. gap becomes
874 approximately linear and equal to the overlap time plus around 100 ms.

875 Fig. 13(d) shows the effect of the dopamine parameter on saccade latencies in gap, step and overlap
876 conditions. In general, the effect of decreasing the dopamine parameter was a smooth, monotonic and
877 undramatic increase in saccade latency. However, the data for the overlap condition with a target luminance
878 which was 3 times as bright as the fixation luminance was more interesting. Here we see a transition around

879 a dopamine value if 0.7. Below this value, the basal ganglia is not able to select the target luminance until
880 the fixation is removed, reducing the excitatory drive from STN to SNr, and consequently the inhibition
881 from SNr to the thalamo-cortical loop. For the target luminance 0.6, 0.7 dopamine allows the basal ganglia
882 to select sufficiently well so that the target can build up in the thalamo-cortical loop, in spite of the fixation
883 overlap.

884 The relationship between latency and the target luminance is given in Fig. 13(e). This shows latency for a
885 100 ms gap, step and 100 ms overlap conditions for a given fixation luminance of 0.2, and a horizontally
886 located target at $\theta_y^t = -10^\circ$. For the gap condition, we see very short latencies for luminances of about
887 0.75 and above. Finally, the activity driving these express saccades is initiated by high firing rates in the
888 superficial layer of SC (SCs), which then drives activity in thalamus and through the basal ganglia. A
889 gradual transition from express saccades to reflexive saccades is observed as the contribution of the SCs
890 becomes weaker and the drive from FEF into the thalamo-cortical loop becomes necessary to elicit a
891 saccade. A similar gradual transition, albeit for higher latencies is seen for the step condition. At higher
892 target luminances, the SCs has a greater effect on the activity in the thalamo-cortical loop. However, the
893 activity in STN caused by the fixation luminance increases the latency at all luminance values compared
894 with the gap condition. The overlap condition leads to increased latencies for luminances below 2.5, but
895 meets the step condition above this value, at which the 0.2 fixation luminance appears to have a negligible
896 effect on the system.

897 3.5 Saccade sequences

898 We now present results derived from the fully parameterised and integrated model; where we took
899 advantage of the fact that it is a closed loop system. This allowed us to present sequences of target
900 luminances and allow the model to direct its fovea at the most salient target.

901 3.5.1 Out & return

902 We investigated the behaviour of the model for saccade sequences. In one experiment, we illuminated
903 a fixation cross from 0 s until 0.4 s, followed by a target at $(0, -10^\circ)$ from 0.4 s until 0.8 s. Finally, the
904 fixation was again shown from 0.8 s until the end of the simulation at 2 s. This induced a saccade to a
905 10° eccentricity, followed by a return saccade back to the null point. We noticed some irregularities in
906 the return saccades, which were accurate, but had a significant overshoot. More perplexingly, if the target
907 was switched repeatedly between 0° and 10° , second and subsequent outward saccades also showed this
908 overshoot. We found that the cause of these irregularities was the lack (in ‘TModel4’) of any mechanism to
909 reset the tonic neurons in the SBG after the first saccade. This resulted in TN activity in the left channel
910 and also in the right channel. Interestingly, this ensured that, at least for a few, consecutive out-and-return
911 saccades, the saccade accuracy was accidentally relatively good, with trajectories resembling experimental
912 data (Bahill and Stark (1979), p. 6). Had the return accuracy not been so accurate, we may have noticed the
913 lack of a tonic neuron reset mechanism and corrected this oversight earlier. Such a mechanism is indeed
914 proposed and included in the connectivity of the Gancarz and Grossberg (1998) model. We implemented
915 this feature by adding an additional inhibitory input to the ‘integrator’ component of TModel4, driven
916 by the contralateral EBN population, naming the new model ‘TModel5’. Now, when the eye is directed
917 towards an eccentric target which is then exchanged with a target at the null point, the EBN activity toward
918 the null point will tend to extinguish the TN activity which was holding the eye at the eccentric position.
919 We verified that none of the single saccade results were affected by this modification.

920 Fig. 14 shows the outward and return trajectories produced by the experiment with the TN reset mechanism.
921 Panel (a) shows the x and y rotation trajectory; panel (b) shows individual rotational components of
922 the eye. Fig. 14(c) shows out and return trajectories for three other saccade targets; horizontal, vertical and
923 oblique. The trajectories have characteristic shapes and also show some stochastic variation caused by the
924 noise in the model [see dashed trajectories in Fig. 14(a)].

925 The return trajectories (magenta lines) showed a distinctly different form from the outward trajectories.
926 They overshot their destination (the null point) significantly. This resulted from the removal of the TN
927 activity which was holding the eye at the eccentric target location. Removal of this activity, and thus the
928 static force exerted by the corresponding extraocular muscle, meant that the eye was subject both to a new
929 muscular force towards the null point *alongside* the restorative spring force of the lengthened rectus muscle.
930 This stands as a shortcoming of the model.

931 3.5.2 Double steps

932 In another experiment, we probed the response of the model to double step stimuli of the type described
933 in Becker and Jrgens (1979). In that work, the response of human subjects was investigated when shown
934 stimuli at 15° and 30° eccentricity with variable delay between the stimuli. If the smaller eccentricity
935 stimulus was shown first, followed by the more distal on the same side of the field of view, this was called
936 a ‘staircase’ presentation. We carried out a ‘staircase’ presentation, shown in Fig. 15, where our small
937 eccentricity luminance was at 8° and our more distal luminance was at 12° (both to the right of centre). **The**
938 **stimuli could not be presented at 15° and 30° to match the experiment, because 30° saccades were outside**
939 **the range of the model.**

940 We found that there was a critical time delay between the luminances of about 30 ms. If they were
941 presented with a delay smaller than this value, then a single, slightly hypermetric saccade was made. This
942 response type is called a *final angle response*. A delay greater than 30 ms between the stimuli would lead to
943 double step saccades (a so-called *initial angle response*), with the first saccade arriving at 8° (though with
944 greater variability than normal), and a second saccade being made to a location hypometric of 12° after a
945 pause of about 240 ms. Fig. 15(a) shows the mean trajectories from 5 simulations of the staircase doublestep
946 presentation alongside the result for a single saccade to the final angle of 12° . Dash-dot lines show ± 1
947 standard deviation about the mean. The corresponding trajectories are shown in Fig. 15(b).

948 Inspection of the activity maps in FEF and SC_deep (not shown) indicates that when the 8° target
949 is illuminated for 30 ms or more, the activity associated with this target angle is able to dominate the
950 activity, hence the execution of a reasonably accurate saccade. The inhibitory feedback from the SBG then
951 extinguishes activity in FEF, thalamus and SC, which means that a full 200 ms or more is required to allow
952 activity in these populations to build up again in order to make the smaller saccade from 8° to 12° . This is
953 in contrast to experimental findings in which the corrective second saccade is often executed *more quickly*
954 than if it were programmed on its own (Becker and Jrgens, 1979).

4 DISCUSSION

955 The aim of this study was to demonstrate the importance of modelling neurological systems *in concert with*
956 the biomechanical systems with which they have evolved. We hypothesised that by combining existing
957 neurophysiological models with an accurate model of a musculo-skeletal system, and then ‘closing the
958 loop’ by allowing the movements of the virtual muscles to modulate sensory feedback to the brain model,

shortcomings in the constituent models would be revealed, leading to new knowledge. We call this closed-loop approach *computational neurobehaviour*, meaning a complete, behaving model, with attention paid to the biological accuracy of each brain and biomechanical sub-system. There already exist many closed-loop *robotic* systems which receive sensory input from the world, process that input and generate behaviour by activating motor systems (Yu et al., 2004; Fend et al., 2004; Pearson et al., 2007). We now consider whether robotic systems which model biological components *in hardware* could fall within our new category. Using a number of examples, we will attempt to illustrate what we mean by computational neurobehaviour. We'll consider which examples fall into the new category and which are covered by other fields of robotics or computational neuroscience.

Pearson et al. (2007) describes a wheeled robot which has a biomimetic whisker sensory system, along with a biomimetic neural system imitating the behaviour of the rat's sensory processing systems and controlling the movement of the robot. Fend et al. (2004) is a similar, wheeled, whiskered robot, with a repertoire of three behaviours organised in a subsumption architecture. In both robots, actions that are selected within the brain model drive a non-biologically accurate wheel motor control algorithm to achieve rotational and translational movements. Although both have sensory and processing systems which are guided by biology, the non-biological motor control stage prevents us from considering these as being studies of computational neurobehaviour. Yu et al. (2004) report on a biomimetic fish robot, whose motor system closely resembles that of the real fish. The robot is able to operate in a closed-loop mode, where sensory input is provided to the non-biomimetic control algorithms from overhead cameras, but its control system is also able to operate in open-loop mode. Neither the control system, nor the sensory system are biophysically accurate and we would not describe this study as computational neurobehaviour. Nevertheless, the biophysically accurate motor system could certainly form part of a computational neurobehavioural study of swimming behaviour in the fish, if it were combined with suitable sensory input and sensory processing models. Knips et al. (2017) is a report of a reach-and-grasp robot arm controlled via a dynamic neural field brain model. The sensory input for this system—its ‘eyes’—is a Microsoft Kinect sensor; it also has somatosensory feedback from the fingers of the robot’s hand. The neural field ‘brain’ controls the seven degrees of freedom of the arm to carry out the reach-and-grasp action. While this robot has closed-loop control and is clearly inspired by biology, it remains a study of robotics and of the improvement of the control of the robot’s reach-and-grasp function, rather than a study which aims to learn more about the biology of a primate arm. For this reason, we would describe the study of Knips et al. (2017) as embodied robotics or neuro-robotics.

Modern programming platforms, often originating from the computer game industry, make it relatively easy to model a virtual environment. Consequently, an increasing number of studies into robotic or neuro-mimetic control are carried out with virtual robots operating within a virtual environment. Arena et al. (2017) describes a robotic insect system based on the fly species *Drosophila Melanogaster*. It has biomimetic insect legs implemented in a virtual robot and a neuro-mimetic brain. Closing the loop is a visual sensory input system which is able to determine the distance between the robot and an obstacle and the obstacle’s height. The visual system is not described in detail and may not be biologically modelled (much in the way that the visual processing stream is not modelled in detail in the present work). Nevertheless, this study may reasonably be described as computational neurobehaviour; the authors demonstrate that the virtual robot is able to learn to climb obstacles in a realistic manner and suggest that the model may be compared with experimental data from future Drosophila experiments addressing obstacle climbing and learning. N’Guyen et al. (2014) and Thurat et al. (2015) are two studies of the oculomotor system which model sensory input, neural control and motor output. These studies fall outside the remit of computational neurobehaviour only because they omit to close the sensory loop. DeWolf et al. (2016) describes a reach

1004 model comprising a simplified virtual arm (with fewere degrees of freedom than a primate arm), and
1005 a biologically inspired brain model. This model also omits to close the sensory feedback loop and we
1006 consider it a traditional computational neuroscience study.

1007 We can now offer a definition of computational neurobehaviour as: *The study of biological sensory-motor*
1008 *system behaviour using biophysically accurate models of sensory input, brain and motor sub-systems*
1009 *operating in a closed-loop*. The sub-system models may be implemented in software or hardware, provided
1010 that they attempt to reproduce and explain features of the biological sub-system. We favour virtual
1011 biomechanics, for the ease with which the biomechanical model can be modified and the flexibility of
1012 computational modelling over hardware modelling.

1013 To demonstrate the validity of the computational neurobehaviour approach, we built an integrated model
1014 and then identified the modifications which were necessary to give it the ability to make accurate movements
1015 under one type of stimulus. We then examined its behaviour with other stimuli. We chose the oculomotor
1016 model as a basis for this study because it has only three degrees of freedom, making it one of the simplest
1017 musculo-skeletal systems. Furthermore, eye movements fall into several well-defined categories, each being
1018 controlled by separate brain circuits, we were therefore justified in modelling a system which produced
1019 only saccadic eye movements. Nevertheless, we are aware that we did not create a complete model of
1020 the system; no treatment of the cerebellum was attempted, justified because cerebellum appears to have
1021 only a minor effect on saccade accuracy (Dean and Porrill, 2008), probably correcting for slow to medium
1022 timescale changes in the physical dynamics of the eyeball (Dean et al., 1994).

1023 To summarise our model integration: We combined the Cope-Chambers model (Cope et al., 2017) with a
1024 saccadic burst generator model based on the work of Gancarz and Grossberg (1998), using this to drive the
1025 input of a new biomechanical eye model. To achieve the spatial transformation from the retinotopic maps of
1026 the Cope-Chambers model to the six ‘muscle channel’ inputs for the saccadic burst generator, we used the
1027 mapping of Ottes et al. (1986) to produce parameterised weight maps along with an empirically discovered
1028 synergy for the torsional weight maps. We introduced an additional transformation to the brain model to
1029 achieve invariant sized hills of activity in superior colliculus to fulfil the invariant integral hypothesis of
1030 Tabareau et al. (2007). We closed the loop using a software component which transformed a view of a
1031 world containing luminous cross shapes into the eye’s frame of reference, given its instantaneous rotational
1032 state. This component also computed the inverse of the mapping from Ottes et al. (1986) to project the
1033 view retinotopically into the brain model. This paper serves to describe how we achieved the integration in
1034 order to test our hypothesis, and we intend that the material and methods section, along with the model
1035 code itself, will help others to carry out similar studies. However, we wish to devote the majority of this
1036 discussion to what can be learned from an integrated model of a combined brain and biomechanical system,
1037 using our oculomotor system as an example.

1038 Our integration approach revealed three ways in which this model fails to provide a full understanding
1039 of the saccadic system. In each case, the issue is made clear *as a result of the integration*. This is not to
1040 say that other approaches may not also reveal shortcomings; we will see that one of our cases has been
1041 independently identified (Groh, 2011).

1042 4.1 The need for a widening projection field

1043 The original combination of the Cope-Chambers model with the theoretical weight maps of Ottes et al.
1044 (1986) and Tabareau et al. (2007) resulted in a model which was able to produce accurate saccades only
1045 along the principle rotational axes (Fig. 10). Thus, *the integration of the models* suggested that an additional
1046 layer was required to achieve accurate saccades for oblique, as well as for horizontal and vertical saccades.

1047 Although the *need* for an invariant integral is discussed in Tabareau et al. (2007) as resulting from their
1048 theoretical study, the mechanism by which such an invariant Gaussian hill is generated is not. By combining
1049 the models, we were forced to consider this mechanism, and hypothesised that a widening projection field
1050 would be a candidate mechanism. The results of Fig. 11 indicate that a substantial improvement in accuracy
1051 is indeed achieved by this new mechanism.

1052 **4.2 Saccades from non-null starting positions**

1053 The implementation of a biophysically accurate model of the eye, and the closed-loop nature of the model
1054 makes it very natural to consider how the model will behave when making saccades from arbitrary starting
1055 positions, or how it would respond to a sequence of stimuli. This was the motivation for the out-and-return
1056 experiment (Fig. 14) as well as for the double step experiment (Fig. 15). We found that return saccades were
1057 substantially affected by the biomechanics of the eye, as the brain and brainstem model had no mechanism
1058 to account for the position-dependent restoring forces applied by the eye. This question has been addressed
1059 by other authors; Groh (2011) investigates the effect of initial eye position on stimulated saccades and finds
1060 a need for the signal in superior colliculus to be modulated by an eye position signal. Ling et al. (2007)
1061 shows the existence of a position dependent firing rate offset in abducens neurons. Though we will not
1062 speculate here on the mechanism by which return saccades may be made accurate whilst also resetting
1063 the activity of tonic neurons in the SBG, it is interesting that in the model in which we omitted to reset
1064 TN activity (TModel4), we obtained relatively accurate out-and-return saccades which closely resembled
1065 experimental data. We suggest that residual activity in TN populations may offer an explanation for how
1066 the restorative force exerted by the elastic oculomotor muscles is compensated for. A comparison of this
1067 idea with that of Groh (2011) (that there is a modulation, from a brainstem signal, of the SC readout) would
1068 make a subject for a future study. Although these existing studies have highlighted this issue, the inaccurate
1069 return saccades which the model makes from eccentric starting positions provide a clear example of the
1070 way in which integrating known models into a closed-loop system can highlight deficiencies in the model.

1071 **4.3 Inhibitory feedback from saccadic burst generator to brain**

1072 The third issue raised by the integration of the component models of the saccadic system has, like
1073 the return saccades, to do with resetting activity. In this case, rather than the reset of activity in the TN
1074 population in the brainstem, it is the question of how the activity in the *brain* model should be reset after
1075 each saccade. When a target luminance is projected onto the World population in the model, this induces
1076 activity which ‘reverberates’ in loops through FEF, basal ganglia, SC and thalamus. The brainstem contains
1077 a mechanism to limit the timescale of a saccade (inhibitory feedback from EBN, via IBN to LLBN; see
1078 Fig. 4). However, if the activity in SC is not reset, then following the completion of the first saccade, a
1079 series of subsequent ‘staircase’ saccades will be executed. There needs to be a mechanism to extinguish
1080 activity in SC, but also in FEF and thalamus, as activity in either of these populations can build up and
1081 eventually cause repeat activity in SC and another saccade. We added hypothetical inhibitory feedback
1082 connections to our model, such that the IBN populations in the SBG would inhibit activity in FEF, thalamus
1083 and SC_deep (Fig. 4), preventing the occurrence of staircase saccades.

1084 An examination of the behaviour of the model when presented with ‘double-step stimuli’ reveals a
1085 problem with our inhibitory feedback connections. We found that when double-step stimuli were presented
1086 (where an initial target at 8° was replaced with a 12° target after 30 or 40 ms) and a double saccade was
1087 made [Fig. 15(a), black lines] the second saccade latency was *longer* even than the initial saccade. This
1088 contrasts with Becker and Jrgens (1979) who find that second, corrective saccades occur with *shorter*
1089 latencies. This suggests that the inhibitory reset signal implemented in this model is too strong or has the

1090 wrong timescales. This issue highlights the fact that connections *between* component models are quite as
1091 important as the connections within each model.

1092 There is some evidence for an inhibitory projection to SC from the brainstem. Corvisier and Hardy
1093 (1991) offer evidence for a projection from the propositus hypoglossi nucleus. This lies upstream from
1094 motoneurons and (in primates) encodes eye velocity (Dale and Cullen, 2013), rather than head movement
1095 velocity. Although the propositus hypoglossi does not lie in exactly the same functional location as our IBN
1096 population (instead it sits between TN and MN), it offers a possible inhibitory feedback signal proportional
1097 to eye velocity and may help to reduce activity in SC post-saccade. Alternatively, it is possible that activity
1098 in FEF and thalamus are reset via a ‘timed signal’. Feasibly, after activity in FEF exceeds a threshold, an
1099 internal, inhibitory feedback signal could be activated. This inhibition should have a timescale of sufficient
1100 duration to reduce activity in FEF, thalamus and, via an increase in inhibitory output from SNr, also in SC.
1101 Indeed, the cortical microcircuit contains a variety of morphologically distinct gabaergic neurons (Douglas
1102 and Martin, 2004) which could fulfil this functionality. A similar mechanism would then be required in SC,
1103 to reset activity generated by direct excitation via the retinal-collicular pathway which generates express
1104 saccades. Again, SC is a multi-layered structure, containing gabaergic interneurons (Munoz and Istvan,
1105 1998; Meredith and Ramoa, 1998; Helms et al., 2004; Sooksawate et al., 2011) and there is mounting
1106 evidence that saccade dynamics are generated within SC (Kaneda et al., 2008; Goossens and van Opstal,
1107 2012; Bayguinov et al., 2015). Thus, a more complex treatment of the SC and FEF regions in the model
1108 may well obviate the need for inhibitory feedback from brainstem to SC, FEF and thalamus.

1109 Considering whether a feedback connection, or internal, recurrent inhibition is responsible for activity-
1110 reset in the brain model raises a more general question about modelling the central nervous system. We
1111 should consider whether inaccuracies within one part of the model may propagate errors through the
1112 closed-loop system that cannot be counteracted by another part of the simulation. There is no way to know,
1113 from integrating sub-systems, which properties hold true, and which are false. However, by integrating
1114 models and examining the behaviour of the combined model, we are presented with the right questions to
1115 ask of the model and the experimental data. In the case of activity-reset, this is to re-assess whether there
1116 exists inhibitory feedback from brainstem to the SC and FEF regions, and to find out how an integrated
1117 model with self-regulatory mechanisms in SC and FEF may perform.

1118 4.4 Concluding remarks

1119 There are also experimental closed-loop approaches to understanding sensorimotor control. Ejaz et al.
1120 (2013) places a fly in a fixed position, and couples it with a free-to-move robot. The sensory input collected
1121 by the robot is projected onto the eyes of the fly, and activity from a selected neuron in the fly’s brain
1122 is used to drive a control system for the robot’s movements. This allows the experimenters to study the
1123 behaviour of the fly’s brain operating in a closed-loop condition that is more natural than the open-loop
1124 condition that many other experimental techniques mandate. The results from closed-loop experiments will
1125 undoubtedly inform future neurobehavioural models.

1126 The omission of the cerebellum will not have escaped the reader’s notice. Whilst many of the nuclei
1127 known to be involved in the production of saccadic eye movements are incorporated within the model,
1128 the cerebellum is not. The cerebellum is known to play an important rôle in saccade programming (Dean
1129 et al., 1994; Schweighofer et al., 1996; Quaia et al., 2000; Kleine, 2003). It may be able to completely
1130 replace the functionality of the colliculus when lesioned (Aizawa and Wurtz, 1998; Lefèvre et al., 1998).
1131 However, this rôle is typically considered to be one of accuracy tuning (Barash et al., 1999; Dean et al.,
1132 1994); operating as an additive model. Furthermore, saccades made by individuals with cerebellar ataxias

1133 perform with only moderate loss of saccade accuracy (Barash et al., 1999; Federighi et al., 2011). Because
1134 we did not address learning in our model, and because our aim was to demonstrate the utility of integrating
1135 brain with biomechanics in order to highlight deficiencies, we considered the omission of the cerebellar
1136 nuclei acceptable in the present work.

1137 We have not addressed the question of saccade duration in this paper. Saccade duration is of interest in
1138 models which produce two (or three) dimensional saccades, because the dynamics of a saccade follow well
1139 known relationships with the saccade eccentricity, regardless of the saccade angle. This causes a problem for
1140 models (such as the present one) for which some of the dynamic behaviour is generated within orthogonal
1141 components. For example, saccade duration increases with target eccentricity. A 10° eccentricity oblique
1142 (45° up and right) saccade is composed (approximately) of a 7° upwards component and a 7° rightwards
1143 component. If the component based model is responsible for the dynamics, then the 10° oblique saccade
1144 would be expected to have the dynamics of a 7° up or 7° right saccade. This is not found in practice, and
1145 the components are said to have been stretched, hence the name for this effect ‘component stretching’. The
1146 Gancarz and Grossberg (1998) model is reported to take account of the component stretching effect via
1147 the OPN neuron population. We did not find this effect in our implementation of the model; the duration
1148 of oblique saccades at a given eccentricity was always substantially different from the duration of the
1149 corresponding purely vertical or horizontal saccade. Because there is a somewhat complicated interplay
1150 between the dynamics of the superior colliculus driving the dynamic system of the SBG, we feel this is
1151 outside the scope of the current work and a subject for a future paper.

1152 This work represents a step forward in the modelling of neuromuscular systems, not because it sig-
1153 nificantly advances any of the constituent models, but because it *integrates* the models into a complete,
1154 *behaving* system. This is not the first integrated brain model composed of separately developed components.
1155 The works of N’Guyen et al. (2014) and Thurat et al. (2015) are both based on an example of a brain model
1156 which drives a simple, second order model of the eye. DeWolf et al. (2016) describes a reach model which
1157 integrates models of cortex and cerebellum to drive a two degree-of-freedom arm model. Both of these
1158 example systems nevertheless operate using ‘curated’ inputs supplied by the modeller.

1159 In contrast, the current work allows the state of the system to determine the input delivered to the model.
1160 The modeller only curates the state of the world at each time point, but the actual input to the model
1161 depends on the eye’s rotational state. This is, to our knowledge, the first model which integrates the brain
1162 with an accurate biophysical system and closes the loop in this way, enabling the system to reproduce
1163 behaviour. As such, it offers a platform for testing more complex saccadic behaviour such as antisaccades
1164 or saccades in the presence of distractor stimuli. We believe that by building closed loop systems which
1165 express behaviour, we, and others will develop a new field of *computational neurobehaviour*, which will
1166 share themes from neuroscience, artificial intelligence, decision science and embodied robotics.

DISCLOSURE/CONFLICT-OF-INTEREST STATEMENT

1167 The authors declare that the research was conducted in the absence of any commercial or financial
1168 relationships that could be construed as a potential conflict of interest.

AUTHOR CONTRIBUTIONS

1169 SJ, AB and AC implemented existing parts of the model in SpineML. AB developed the saccade generator
1170 brainstem model. SJ performed the technical and scientific integration of the biomechanical eye. CP and

1171 KM developed the biomechanical eye model. SJ wrote the manuscript; SA, AB, KG and KM contributed
1172 to the manuscript. KG conceived the project.

ACKNOWLEDGEMENTS

1173 *Funding:* European Union FP7 Grant 610391 ‘NoTremor’.

SUPPLEMENTAL DATA

1174 The model specification, results and all code required to reproduce the results of this work are available at:
1175 https://github.com/ABRG-Models/OMM_NeuroMuscular

REFERENCES

- 1176 Aizawa, H. and Wurtz, R. H. (1998). Reversible inactivation of monkey superior colliculus. I. Curvature of
1177 saccadic trajectory. *Journal of neurophysiology* 79, 2082–2096
- 1178 Alex Cope and Paul Richmond (2014). SpineML. RRID: SCR_015641
- 1179 Anderson, R. W., Keller, E. L., Gandhi, N. J., and Das, S. (1998). Two-dimensional saccade-related
1180 population activity in superior colliculus in monkey. *Journal of Neurophysiology* 80, 798–817
- 1181 Arai, K., Keller, E., and Edelman, J. (1994). Two-dimensional neural network model of the primate
1182 saccadic system. *Neural Networks* 7, 1115. doi:10.1016/S0893-6080(05)80162-5
- 1183 Arai, K. and Keller, E. L. (2005). A model of the saccade-generating system that accounts for trajectory
1184 variations produced by competing visual stimuli. *Biological cybernetics* 92, 21–37. doi:10.1007/
1185 s00422-004-0526-y
- 1186 Arena, E., Arena, P., Strauss, R., and Patané, L. (2017). Motor-Skill Learning in an Insect Inspired
1187 Neuro-Computational Control System. *Frontiers in Neurorobotics* 11. doi:10.3389/fnbot.2017.00012
- 1188 Bahill, A. T. and Stark, L. (1979). The trajectories of saccadic eye movements. *Scientific American* 240,
1189 108–117
- 1190 Barash, S., Melikyan, A., Sivakov, A., Zhang, M., Glickstein, M., and Thier, P. (1999). Saccadic dysmetria
1191 and adaptation after lesions of the cerebellar cortex. *Journal of Neuroscience* 19, 10931–10939
- 1192 Bayguinov, P. O., Ghitani, N., Jackson, M. B., and Basso, M. A. (2015). A Hard-Wired Priority Map
1193 in the Superior Colliculus Shaped by Asymmetric Inhibitory Circuitry. *Journal of Neurophysiology*
1194 doi:10.1152/jn.00144.2015
- 1195 Becker, W. and Jrgens, R. (1979). An analysis of the saccadic system by means of double step stimuli.
1196 *Vision Research* 19, 967–983. doi:10.1016/0042-6989(79)90222-0
- 1197 Bevan, M. D. and Wilson, C. J. (1999). Mechanisms underlying spontaneous oscillation and rhythmic
1198 firing in rat subthalamic neurons. *The Journal of neuroscience : the official journal of the Society for
1199 Neuroscience* 19, 7617–28
- 1200 Blenkinsop, A., Anderson, S., and Gurney, K. (2017). Frequency and function in the basal ganglia: the
1201 origins of beta and gamma band activity. *The Journal of Physiology* doi:10.1113/JP273760
- 1202 Bogacz, R. and Gurney, K. (2007). The basal ganglia and cortex implement optimal decision making
1203 between alternative actions. *Neural Computation* 19, 442–477. doi:10.1162/neco.2007.19.2.442
- 1204 Bolam, J., Hanley, J., Booth, P., and Bevan, M. (2000). Synaptic organisation of the basal ganglia. *Journal
1205 of Anatomy* 196, 527–542

- 1206 Brown, P., Oliviero, A., Mazzone, P., Insola, A., Tonali, P., and Di Lazzaro, V. (2001). Dopamine
1207 Dependency of Oscillations between Subthalamic Nucleus and Pallidum in Parkinson's Disease. *J.
1208 Neurosci.* 21, 1033–1038
- 1209 Bruce, C. J. and Goldberg, M. E. (1985). Primate frontal eye fields. I. Single neurons discharging before
1210 saccades. *Journal of Neurophysiology* 53, 603–635
- 1211 Casteau, S. and Vitu, F. (2012). On the effect of remote and proximal distractors on saccadic behavior: A
1212 challenge to neural-field models. *Journal of vision* 12, 14
- 1213 Chambers, J. M., Gurney, K., Humphries, M., and Prescott, A. (2012). Mechanisms of choice in the
1214 primate brain: a quick look at positive feedback. In *Modelling Natural Action Selection* (Cambridge
1215 University Press). 390–420
- 1216 Chen, L. L. and Wise, S. P. (1995). Supplementary eye field contrasted with the frontal eye field during
1217 acquisition of conditional oculomotor associations. *Journal of Neurophysiology* 73, 1122–1134
- 1218 Chevalier, G. and Deniau, J. M. (1990). Disinhibition as a basic process in the expression of striatal
1219 functions. *Trends in Neurosciences* 13, 277–280
- 1220 Cohen, J. Y., Heitz, R. P., Woodman, G. F., and Schall, J. D. (2009). Neural basis of the set-size effect in
1221 frontal eye field: timing of attention during visual search. *Journal of Neurophysiology* 101, 1699–1704.
1222 doi:10.1152/jn.00035.2009
- 1223 Cope, A., Chambers, J. M., Prescott, T. J., and Gurney, K. N. (2017). Basal Ganglia Control Of
1224 Reflexive Saccades: A Computational Model Integrating Physiology Anatomy And Behaviour. *bioRxiv*
1225 doi:10.1101/135251
- 1226 Cope, A. and Gurney, K. N. (2011). A biologically based model of active vision. In *Proceedings of
1227 AISB'11 - Architectures for Active Vision*, eds. S. O'Keefe, Kazakov, D., and Tsoulas, D. (York, UK),
1228 13–20
- 1229 Cope, A. J. and James, S. S. (2015). SpineML_2_brahms (NoTremor Oculomotor branch)
- 1230 Cope, A. J., Richmond, P., and Allerton, D. (2014). The SpineML toolchain: enabling computational neu-
1231 roscience through flexible tools for creating, sharing, and simulating neural models. *BMC Neuroscience*
1232 15, P224
- 1233 Cope, A. J., Richmond, P., and James, S. S. (2015). SpineCreator. RRID: SCR_015637
- 1234 Cope, A. J., Richmond, P., James, S. S., Gurney, K., and Allerton, D. J. (2016). SpineCreator: a
1235 Graphical User Interface for the Creation of Layered Neural Models. *Neuroinformatics* doi:10.1007/
1236 s12021-016-9311-z
- 1237 Corvisier, J. and Hardy, O. (1991). Possible excitatory and inhibitory feedback to the superior colliculus: a
1238 combined retrograde and immunocytochemical study in the prepositus hypoglossi nucleus of the guinea
1239 pig. *Neuroscience Research* 12, 486–502. doi:10.1016/S0168-0102(09)80002-3
- 1240 Dale, A. and Cullen, K. E. (2013). The nucleus prepositus predominantly outputs eye movement-
1241 related information during passive and active self-motion. *Journal of Neurophysiology* 109, 1900.
1242 doi:10.1152/jn.00788.2012
- 1243 Daniel, P. M. and Whitteridge, D. (1961). The representation of the visual field on the cerebral cortex in
1244 monkeys. *The Journal of Physiology* 159, 203–221. doi:10.1113/jphysiol.1961.sp006803
- 1245 Dean, P. (1995). Modelling the role of the cerebellar fastigial nuclei in producing accurate saccades: the
1246 importance of burst timing. *Neuroscience* 68, 1059–1077
- 1247 Dean, P., Mayhew, J. E., and Langdon, P. (1994). Learning and maintaining saccadic accuracy: a model of
1248 brainstemcerebellar interactions. *Journal of Cognitive Neuroscience* 6, 117–138
- 1249 Dean, P. and Porritt, J. (2008). Adaptive filter models of the cerebellum: computational analysis. *Cerebellum*
1250 7, 567–571

- 1251 Delgado, A., Sierra, A., Querejeta, E., Valdiosera, R., and Aceves, J. (1999). Inhibitory control of the
1252 GABAergic transmission in the rat neostriatum by D2 dopamine receptors. *Neuroscience* 95, 1043–1048.
1253 doi:10.1016/S0306-4522(99)00495-9
- 1254 DeLong, M., Crutcher, M. D., and Georgopoulos, A. (1985). Primate globus pallidus and subthalamic
1255 nucleus: functional organization. *Journal of Neurophysiology* 53, 530–543
- 1256 Deubel, H. and Schneider, W. X. (1996). Saccade target selection and object recognition: Evidence for a
1257 common attentional mechanism. *Vision Research* 36, 1827–1837. doi:10.1016/0042-6989(95)00294-4
- 1258 DeWolf, T., Stewart, T. C., Slotine, J.-J., and Eliasmith, C. (2016). A spiking neural model of adaptive arm
1259 control. *Proceedings of the Royal Society B: Biological Sciences* 283, 20162134. doi:10.1098/rspb.2016.
1260 2134
- 1261 Dorris, M. C., Paré, M., and Munoz, D. P. (1997). Neuronal Activity in Monkey Superior Colliculus
1262 Related to the Initiation of Saccadic Eye Movements. *The Journal of Neuroscience* 17, 8566
- 1263 Douglas, R. J. and Martin, K. A. C. (2004). Neuronal Circuits of the Neocortex. *Annual Review of
1264 Neuroscience* 27, 419–451. doi:10.1146/annurev.neuro.27.070203.144152
- 1265 Edelman, J. A. and Keller, E. L. (1996). Activity of visuomotor burst neurons in the superior colliculus
1266 accompanying express saccades. *Journal of Neurophysiology* 76, 908
- 1267 Ejaz, N., Krapp, H. G., and Tanaka, R. J. (2013). Closed-loop response properties of a visual interneuron
1268 involved in fly optomotor control. *Frontiers in Neural Circuits* 7. doi:10.3389/fncir.2013.00050
- 1269 Federighi, P., Cevenini, G., Dotti, M. T., Rosini, F., Pretegiani, E., Federico, A., et al. (2011). Differences
1270 in saccade dynamics between spinocerebellar ataxia 2 and late-onset cerebellar ataxias. *Brain* 134,
1271 879–891. doi:10.1093/brain/awr009
- 1272 Fend, M., Bovet, S., and Hafner, V. (2004). The artificial mouse-a robot with whiskers and vision.
1273 *Proceedings of the 35th International Symposium on Robotics, Paris, 2004.*, 1–6
- 1274 Fuchs, A. and Luschei, E. (1970). Firing patterns of abducens neurons of alert monkeys in relationship to
1275 horizontal eye movement. *Journal of Neurophysiology* 33, 382–392
- 1276 Funahashi, S., Chafee, M. V., and Goldman-Rakic, P. S. (1993). Prefrontal neuronal activity in rhesus
1277 monkeys performing a delayed anti-saccade task. *Nature* 365, 753
- 1278 Galvan, A. and Wichmann, T. (2008). Pathophysiology of Parkinsonism. *Clinical Neurophysiology* 119,
1279 1459–1474. doi:10.1016/j.clinph.2008.03.017
- 1280 Gancarz, G. and Grossberg, S. (1998). A neural model of the saccade generator in the reticular formation.
1281 *Neural Networks* 11, 1159–1174. doi:10.1016/S0893-6080(98)00096-3
- 1282 Gaymard, B., Ploner, C. J., Rivaud, S., Vermersch, A. I., and Pierrot-Deseilligny, C. (1998). Cortical
1283 control of saccades. *Experimental Brain Research* 123, 159–163. doi:10.1007/s002210050557
- 1284 Gerfen, C. R., Engbar, T. M., Mahan, L. C., Susel, Z., Chase, T. N., Monsma, F. J., et al. (1990). D1 and
1285 D2 dopamine receptor regulated gene-expression of striatonigral and striatopallidal neurons. *Science*
1286 250, 1429–1432
- 1287 Ghitani, N., Bayguinov, P. O., Vokoun, C. R., McMahon, S., Jackson, M. B., and Basso, M. A. (2014).
1288 Excitatory Synaptic Feedback from the Motor Layer to the Sensory Layers of the Superior Colliculus.
1289 *The Journal of Neuroscience* 34, 6822–6833. doi:10.1523/JNEUROSCI.3137-13.2014
- 1290 Gian G. Mascetti and Jorge R. Arriagada (1981). Tectotectal interactions through the commissure of the
1291 superior colliculi. An electrophysiological study. *Experimental Neurology* 71, 122–133
- 1292 Girard, B. and Berthoz, A. (2005). From brainstem to cortex: Computational models of saccade generation
1293 circuitry. *Progress in Neurobiology* 77, 215–251. doi:10.1016/j.pneurobio.2005.11.001
- 1294 Goldberg, M. E. and Wurtz, R. H. (1972). Activity of superior colliculus in behaving monkey. I. Visual
1295 receptive fields of single neurons. *J Neurophysiol* 35, 542–559

- 1296 Gonon, F. (1997). Prolonged and extrasynaptic excitatory action of dopamine mediated by D1 receptors in
1297 the rat striatum in vivo. *The Journal of neuroscience : the official journal of the Society for Neuroscience*
1298 17, 5972–8
- 1299 Goossens, H. (2006). Dynamic Ensemble Coding of Saccades in the Monkey Superior Colliculus. *Journal*
1300 *of Neurophysiology* 95, 2326–2341. doi:10.1152/jn.00889.2005
- 1301 Goossens, H. and van Opstal, A. J. (2012). Optimal control of saccades by spatial-temporal activity patterns
1302 in the monkey superior colliculus. *PLoS computational biology* 8, e1002508
- 1303 Groh, J. M. (2001). Converting neural signals from place codes to rate codes. *Biological cybernetics* 85,
1304 159–165
- 1305 Groh, J. M. (2011). Effects of Initial Eye Position on Saccades Evoked by Microstimulation in the Primate
1306 Superior Colliculus: Implications for Models of the SC Read-Out Process. *Frontiers in Integrative*
1307 *Neuroscience* 4. doi:10.3389/fnint.2010.00130
- 1308 Gurney, K., Prescott, T. J., and Redgrave, P. (2001a). A computational model of action selection in the
1309 basal ganglia. I. A new functional anatomy. *Biological cybernetics* 84, 401–10
- 1310 Gurney, K., Prescott, T. J., and Redgrave, P. (2001b). A computational model of action selection in the
1311 basal ganglia. II. Analysis and simulation of behaviour. *Biological cybernetics* 84, 411–23
- 1312 Hallworth, N. E., Wilson, C. J., and Bevan, M. D. (2003). Apamin-sensitive small conductance calcium-
1313 activated potassium channels, through their selective coupling to voltage-gated calcium channels, are
1314 critical determinants of the precision, pace, and pattern of action potential generation in rat subthalamic
1315 nucleus neurons in vitro. *The Journal of neuroscience* 23, 7525–7542
- 1316 Harsing, L. G. and Zigmond, M. J. (1997). Influence of dopamine on GABA release in striatum: evidence
1317 for D1-D2 interactions and non-synaptic influences. *Neuroscience* 77, 419–29
- 1318 Hazy, T. E., Frank, M. J., and O'Reilly, R. C. (2007). Towards an executive without a homunculus:
1319 computational models of the prefrontal cortex/basal ganglia system. *Philosophical Transactions of the*
1320 *Royal Society B: Biological Sciences* 362, 1601–1613. doi:10.1098/rstb.2007.2055
- 1321 Helms, M. C., Özen, G., and Hall, W. C. (2004). Organization of the Intermediate Gray Layer of the
1322 Superior Colliculus. I. Intrinsic Vertical Connections. *Journal of Neurophysiology* 91, 1706–1715.
1323 doi:10.1152/jn.00705.2003
- 1324 Hepp, K. and Henn, V. (1983). Spatio-temporal recoding of rapid eye movement signals in the monkey
1325 paramedian pontine reticular formation (PPRF). *Experimental brain research* 52, 105–120
- 1326 Hepp, K., Van Opstal, A. J., Straumann, D., Hess, B. J., and Henn, V. (1993). Monkey superior colliculus
1327 represents rapid eye movements in a two-dimensional motor map. *Journal of neurophysiology* 69,
1328 965–979
- 1329 Hernández-López, S., Bargas, J., Surmeier, D. J., Reyes, A., and Galarraga, E. (1997). D1 receptor
1330 activation enhances evoked discharge in neostriatal medium spiny neurons by modulating an L-type
1331 Ca²⁺ conductance. *The Journal of neuroscience : the official journal of the Society for Neuroscience* 17,
1332 3334–42
- 1333 Hikosaka, O., Takikawa, Y., and Kawagoe, R. (2000). Role of the basal ganglia in the control of purposive
1334 saccadic eye movements. *Physiological reviews* 80, 953–978
- 1335 Hikosaka, O. and Wurtz, R. H. (1983). Visual and oculomotor functions of monkey substantia nigra
1336 pars reticulata. IV. Relation of substantia nigra to superior colliculus. *Journal of neurophysiology* 49,
1337 1285–301
- 1338 Howard, L. A. and Tipper, S. (1997). Hand deviations away from visual cues: indirect evidence for
1339 inhibition. *Experimental brain research* 113, 144–152

- 1340 Humphries, M. D. and Gurney, K. N. (2002). The role of intra-thalamic and thalamocortical circuits in
1341 action selection. *Network: Computation in Neural Systems* 13, 131–156
- 1342 INCF Task Force on Multi-Scale Modeling (2011). Network Interchange for Neuroscience Modeling
1343 Language (NineML)
- 1344 Isa, T. (2002). Intrinsic processing in the mammalian superior colliculus. *Current Opinion in Neurobiology*
1345 12, 668–677. doi:10.1016/S0959-4388(02)00387-2
- 1346 Isa, T. and Hall, W. C. (2009). Exploring the Superior Colliculus In Vitro. *Journal of Neurophysiology*
1347 102, 2581–2593. doi:10.1152/jn.00498.2009
- 1348 James, S., Bell, O. A., Nazli, M. A. M., Pearce, R. E., Spencer, J., Tyrrell, K., et al. (2017). Target-distractor
1349 synchrony affects performance in a novel motor task for studying action selection. *PLOS ONE* 12,
1350 e0176945. doi:10.1371/journal.pone.0176945
- 1351 Jayaraman, A., Batton, R. R., and Carpenter, M. B. (1977). Nigrotectal projections in the monkey: an
1352 autoradiographic study. *Brain research* 135, 147–152
- 1353 Jiang, H., Stein, B. E., and McHaffie, J. G. (2003). Opposing basal ganglia processes shape midbrain
1354 visuomotor activity bilaterally. *Nature* 423, 982–986. doi:10.1038/nature01698
- 1355 Kaneda, K., Phongphanphanee, P., Katoh, T., Isa, K., Yanagawa, Y., Obata, K., et al. (2008). Regulation of
1356 Burst Activity through Presynaptic and Postsynaptic GABAB Receptors in Mouse Superior Colliculus.
1357 *Journal of Neuroscience* 28, 816–827. doi:10.1523/JNEUROSCI.4666-07.2008
- 1358 Kita, H. and Kitai, S. T. (1991). Intracellular study of rat globus pallidus neurons: membrane properties
1359 and responses to neostriatal, subthalamic and nigral stimulation. *Brain research* 564, 296–305
- 1360 Kleine, J. F. (2003). Saccade-Related Neurons in the Primate Fastigial Nucleus: What Do They Encode?
1361 *Journal of Neurophysiology* 90, 3137–3154. doi:10.1152/jn.00021.2003
- 1362 Knips, G., Zibner, S. K. U., Reimann, H., and Schöner, G. (2017). A Neural Dynamic Architecture for
1363 Reaching and Grasping Integrates Perception and Movement Generation and Enables On-Line Updating.
1364 *Frontiers in Neurorobotics* 11. doi:10.3389/fnbot.2017.00009
- 1365 Khn, A. A., Williams, D., Kupsch, A., Limousin, P., Hariz, M., Schneider, G.-H., et al. (2004). Event-
1366 related beta desynchronization in human subthalamic nucleus correlates with motor performance. *Brain*
1367 : a journal of neurology 127, 735–46. doi:10.1093/brain/awh106
- 1368 Latto, R. (1977). The effects of bilateral frontal eye-field, posterior parietal or superior collicular lesions
1369 on brightness thresholds in the rhesus monkey. *Neuropsychologia* 15, 507–516
- 1370 Lee, C., Rohrer, W. H., and Sparks, D. L. (1988). Population coding of saccadic eye movements by neurons
1371 in the superior colliculus. *Nature* 332, 357–360. doi:10.1038/332357a0
- 1372 Lefèvre, P., Quaia, C., and Optican, L. M. (1998). Distributed model of control of saccades by superior
1373 colliculus and cerebellum. *Neural Networks* 11, 1175–1190
- 1374 Linden, R. and Perry, V. (1983). Massive retinotectal projection in rats. *Brain research* 272, 145–149
- 1375 Ling, L., Fuchs, A. F., Siebold, C., and Dean, P. (2007). Effects of initial eye position on saccade-related
1376 behavior of abducens nucleus neurons in the primate. *Journal of Neurophysiology* 98, 3581–3599
- 1377 Lynch, J. C., Hoover, J. E., and Strick, P. L. (1994). Input to the primate frontal eye field from the substantia
1378 nigra, superior colliculus, and dentate nucleus demonstrated by transneuronal transport. *Experimental*
1379 *Brain Research* 100, 181–186
- 1380 Maes, P. (1989). *The dynamics of action selection* (Artificial Intelligence Laboratory, Vrije Universiteit
1381 Brussel)
- 1382 Marcos, E. and Genovesio, A. (2016). Determining Monkey Free Choice Long before the Choice Is Made:
1383 The Principal Role of Prefrontal Neurons Involved in Both Decision and Motor Processes. *Frontiers in*
1384 *Neural Circuits* 10. doi:10.3389/fncir.2016.00075

- 1385 Marino, R. A., Trappenberg, T. P., Dorris, M., and Munoz, D. P. (2012). Spatial Interactions in the Superior
1386 Colliculus Predict Saccade Behavior in a Neural Field Model. *Journal of Cognitive Neuroscience* 24,
1387 315–336. doi:10.1162/jocn_a_00139
- 1388 Massone, L. L. E. (1994). A neural-network system for control of eye movements: basic mechanisms.
1389 *Biological Cybernetics* 71, 293–305. doi:10.1007/BF00239617
- 1390 Mays, L. E. and Sparks, D. L. (1980). Dissociation of visual and saccade-related responses in superior
1391 colliculus neurons. *Journal of Neurophysiology* 43, 207–232
- 1392 McCarthy, M. M., Moore-Kochlacs, C., Gu, X., Boyden, E. S., Han, X., and Kopell, N. (2011). Striatal
1393 origin of the pathologic beta oscillations in Parkinson's disease. *Proceedings of the National Academy
1394 of Sciences* 108, 11620–11625. doi:10.1073/pnas.1107748108
- 1395 McFarland, N. R. and Haber, S. N. (2002). Thalamic relay nuclei of the basal ganglia form both reciprocal
1396 and nonreciprocal cortical connections, linking multiple frontal cortical areas. *Journal of Neuroscience*
1397 22, 8117–8132
- 1398 McIlwain, J. T. (1982). Lateral spread of neural excitation during microstimulation in intermediate gray
1399 layer of cat's superior colliculus. *Journal of Neurophysiology* 47, 167–178
- 1400 McPeek, R. M. (2006). Incomplete Suppression of Distractor-Related Activity in the Frontal Eye Field
1401 Results in Curved Saccades. *Journal of Neurophysiology* 96, 2699–2711. doi:10.1152/jn.00564.2006
- 1402 McPeek, R. M., Han, J. H., and Keller, E. L. (2003). Competition Between Saccade Goals in the Superior
1403 Colliculus Produces Saccade Curvature. *Journal of Neurophysiology* 89, 2577–2590. doi:10.1152/jn.
1404 00657.2002
- 1405 McPeek, R. M. and Keller, E. L. (2002). Saccade Target Selection in the Superior Colliculus During a
1406 Visual Search Task. *Journal of Neurophysiology* 88, 2019–2034
- 1407 Meredith, M. A. and Ramoa, A. S. (1998). Intrinsic Circuitry of the Superior Colliculus: Pharmacophysio-
1408 logical Identification of Horizontally Oriented Inhibitory Interneurons. *Journal of Neurophysiology* 79,
1409 1597–1602
- 1410 Middleton, F. A. and Strick, P. L. (2000). Basal ganglia and cerebellar loops: motor and cognitive circuits.
1411 *Brain Research Reviews* 31, 236–250. doi:10.1016/S0165-0173(99)00040-5
- 1412 Mink, J. (1996). The basal ganglia: Focused selection and inhibition of competing motor programs.
1413 *Progress in Neurobiology* 50, 381–425
- 1414 Mink, J. W. and Thach, W. T. (1993). Basal ganglia intrinsic circuits and their role in behavior. *Current
1415 opinion in Neurobiology* 3, 950–957
- 1416 Mitchinson, B., Chan, T.-S., Chambers, J., Pearson, M., Humphries, M., Fox, C., et al. (2010). BRAHMS:
1417 Novel middleware for integrated systems computation. *Advanced Engineering Informatics* 24, 49–61.
1418 doi:10.1016/j.aei.2009.08.002
- 1419 Mitchinson, B. and James, S. S. (2015). BRAHMS. RRID: SCR_015642
- 1420 Monosov, I. E., Trageser, J. C., and Thompson, K. G. (2008). Measurements of simultaneously recorded
1421 spiking activity and local field potentials suggest that spatial selection emerges in the frontal eye field.
1422 *Neuron* 57, 614–625
- 1423 Morén, J., Shibata, T., and Doya, K. (2013). The Mechanism of Saccade Motor Pattern Generation
1424 Investigated by a Large-Scale Spiking Neuron Model of the Superior Colliculus. *PLoS ONE* 8, e57134.
1425 doi:10.1371/journal.pone.0057134
- 1426 Munoz, D. P. (2002). Commentary: Saccadic eye movements: overview of neural circuitry. In *Progress in
1427 Brain Research*, ed. D. M. J. Hyona, W. Heide and R. Radach (Elsevier), vol. Volume 140. 89–96
- 1428 Munoz, D. P. and Everling, S. (2004). Look away: the anti-saccade task and the voluntary control of eye
1429 movement. *Nature Reviews Neuroscience* 5, 218–228. doi:10.1038/nrn1345

- 1430 Munoz, D. P. and Istvan, P. J. (1998). Lateral inhibitory interactions in the intermediate layers of the
1431 monkey superior colliculus. *Journal of Neurophysiology* 79, 1193–1209
- 1432 Nambu, A., Yoshida, S.-i., and Jinnai, K. (1990). Discharge patterns of pallidal neurons with input from
1433 various cortical areas during movement in the monkey. *Brain Research* 519, 183–191. doi:10.1016/
1434 0006-8993(90)90076-N
- 1435 N'Guyen, S., Thurat, C., and Girard, B. (2014). Saccade learning with concurrent cortical and subcortical
1436 basal ganglia loops. *Frontiers in Computational Neuroscience* 8. doi:10.3389/fncom.2014.00048
- 1437 Norman, D. A. and Shallice, T. (1986). Attention to action. In *Consciousness and self-regulation* (Springer).
1438 1–18
- 1439 Nowotny, T. (2011). Flexible neuronal network simulation framework using code generation for NVidia®
1440 CUDA™. *BMC Neuroscience* 12, P239. doi:10.1186/1471-2202-12-S1-P239
- 1441 Nowotny, T., Cope, A. J., Yavuz, E., Stemberg, M., Goodman, D. F., Marshall, J., et al. (2014). SpineML
1442 and Brian 2.0 interfaces for using GPU enhanced Neuronal Networks (GeNN). *BMC Neuroscience* 15,
1443 P148. doi:10.1186/1471-2202-15-S1-P148
- 1444 Olivier, E., Corvisier, J., Pauluis, Q., and Hardy, O. (2000). Evidence for glutamatergic tectotectal neurons
1445 in the cat superior colliculus: a comparison with GABAergic tectotectal neurons. *European Journal of
1446 Neuroscience* 12, 2354–2366
- 1447 Ottes, F. P., Van Gisbergen, J. A., and Eggermont, J. J. (1986). Visuomotor fields of the superior colliculus:
1448 A quantitative model. *Vision Research* 26, 857–873. doi:10.1016/0042-6989(86)90144-6
- 1449 Papapavlou, C. and Moustakas, K. (2014). Physics-based modelling and animation of saccadic eye
1450 movement
- 1451 Parent, A. and Hazrati, L. (1993). Anatomical aspects of information processing in primate basal ganglia.
1452 *Trends in Neuroscience* 16, 111–116
- 1453 Pearson, M. J., Pipe, A. G., Melhuish, C., Hutchinson, B., and Prescott, T. J. (2007). Whiskerbot: A robotic
1454 active touch system modeled on the rat whisker sensory system. *Adaptive Behaviour* 15
- 1455 Quaia, C., Lefèvre, P., and Optican, L. M. (1999). Model of the Control of Saccades by Superior Colliculus
1456 and Cerebellum. *Journal of Neurophysiology* 82, 999
- 1457 Quaia, C., Paré, M., Wurtz, R. H., and Optican, L. M. (2000). Extent of compensation for variations
1458 in monkey saccadic eye movements. *Experimental Brain Research* 132, 39–51. doi:10.1007/s002219900324
- 1459 Redgrave, P., Prescott, T. J., and Gurney, K. (1999). The basal ganglia: a vertebrate solution to the selection
1460 problem? *Neuroscience* 89, 1009–1023
- 1461 Reppert, T. R., Lempert, K. M., Glimcher, P. W., and Shadmehr, R. (2015). Modulation of Saccade
1462 Vigor during Value-Based Decision Making. *Journal of Neuroscience* 35, 15369–15378. doi:10.1523/
1463 JNEUROSCI.2621-15.2015
- 1464 Reulen, J. P. H. (1984). Latency of visually evoked saccadic eye movements. *Biological Cybernetics* 50,
1465 251–262. doi:10.1007/BF00337075
- 1466 Richmond, P. (2015). DAMSON
- 1467 Richmond, P., Cope, A., Gurney, K., and Allerton, D. J. (2014). From Model Specification to Simulation
1468 of Biologically Constrained Networks of Spiking Neurons. *Neuroinformatics* 12, 307–323. doi:10.1007/
1469 s12021-013-9208-z
- 1470 Robinson, D. (1972). Eye movements evoked by collicular stimulation in the alert monkey. *Vision Research*
1471 12, 1795–1808. doi:10.1016/0042-6989(72)90070-3
- 1472 Robinson, D. A. (1975). Oculomotor control signals. In *Basic mechanisms of ocular motility and their
1473 clinical implications*, eds. G. Lennerstrand and P. Bach-y Rita (Oxford: Pergamon). 337–374

- 1475 Robinson, D. A. and Fuchs, A. F. (1969). Eye movements evoked by stimulation of frontal eye fields.
1476 *Journal of Neurophysiology* 32, 637–648
- 1477 Rovamo, J. and Virsu, V. (1979). An estimation and application of the human cortical magnification factor.
1478 *Experimental Brain Research* 37, 495–510. doi:10.1007/BF00236819
- 1479 Sabes, P. N., Breznen, B., and Andersen, R. A. (2002). Parietal representation of object-based saccades.
1480 *Journal of Neurophysiology* 88, 1815–1829
- 1481 Saint-Cyr, J. A., Ungerleider, L. G., and Desimone, R. (1990). Organization of visual cortical inputs to the
1482 striatum and subsequent outputs to the pallidonigral complex in the monkey. *Journal of Comparative
1483 Neurology* 298, 129–156
- 1484 Schall, J. D., Hanes, D. P., Thompson, K. G., and King, D. J. (1995). Saccade target selection in frontal
1485 eye field of macaque .1. Visual and premovement activation. *Journal of Neuroscience* 15, 6905–6918
- 1486 Schall, J. D. and Thompson, K. G. (1999). Neural selection and control of visually guided eye movements.
1487 *Annual review of neuroscience* 22, 241–259
- 1488 Schiller, P. H., Sandell, J. H., and Maunsell, J. H. (1987). The effect of frontal eye field and superior
1489 colliculus lesions on saccadic latencies in the rhesus monkey. *Journal of Neurophysiology* 57, 1033
- 1490 Schlag, J. D. (2002). Neurons that program what to do and in what order. *Neuron* 34, 177–178
- 1491 Schwartz, E. L. (1977). Spatial mapping in the primate sensory projection: Analytic structure and relevance
1492 to perception. *Biological Cybernetics* 25, 181–194. doi:10.1007/BF01885636
- 1493 Schwartz, E. L. (1980). Computational anatomy and functional architecture of striate cortex: A spatial
1494 mapping approach to perceptual coding. *Vision Res.* 20, 645–669
- 1495 Schweighofer, N., Arbib, M. A., and Dominey, P. F. (1996). A model of the cerebellum in adaptive control
1496 of saccadic gain. *Biological Cybernetics* 75, 19–28
- 1497 Scudder, C. A. (1988). A new local feedback model of the saccadic burst generator. *J Neurophysiol* 59,
1498 1454
- 1499 Segraves, M. A. and Goldberg, M. E. (1987). Functional properties of corticotectal neurons in the monkey's
1500 frontal eye field. *Journal of Neurophysiology* 58, 1387–1419
- 1501 Seth, A., Sherman, M., Reinbolt, J. a., and Delp, S. L. (2011). OpenSim: a musculoskeletal modeling
1502 and simulation framework for in silico investigations and exchange. *Procedia IUTAM* 2, 212–232.
1503 doi:10.1016/j.piutam.2011.04.021
- 1504 Slotnick, S. D., Klein, S. A., Carney, T., and Sutter, E. E. (2001). Electrophysiological estimate of human
1505 cortical magnification. *Clinical Neurophysiology* 112, 1349–1356
- 1506 Sommer, M. A. and Wurtz, R. H. (2000). Composition and topographic organization of signals sent from
1507 the frontal eye field to the superior colliculus. *Journal of Neurophysiology* 83, 1979–2001
- 1508 Sooksawate, T., Isa, K., Behan, M., Yanagawa, Y., and Isa, T. (2011). Organization of GABAergic
1509 inhibition in the motor output layer of the superior colliculus. *European Journal of Neuroscience* 33,
1510 421–432. doi:10.1111/j.1460-9568.2010.07535.x
- 1511 Sparks, D. L. (2002). The brainstem control of saccadic eye movements. *Nature Reviews Neuroscience* 3,
1512 952–964. doi:10.1038/nrn986
- 1513 Sparks, D. L. and Nelson, I. S. (1987). Sensory and motor maps in the mammalian superior colliculus.
1514 *Trends in Neurosciences* 10, 312–317. doi:10.1016/0166-2236(87)90085-3
- 1515 Stanton, G. B., Goldberg, M. E., and Bruce, C. J. (1988a). Frontal eye field efferents in the macaque
1516 monkey: I. Subcortical pathways and topography of striatal and thalamic terminal fields. *Journal of
1517 Comparative Neurology* 271, 473–492. doi:10.1002/cne.902710402

- 1518 Stanton, G. B., Goldberg, M. E., and Bruce, C. J. (1988b). Frontal eye field efferents in the macaque
1519 monkey: II. Topography of terminal fields in midbrain and pons. *The Journal of Comparative Neurology*
1520 271, 493–506. doi:10.1002/cne.902710403
- 1521 Sterling, P. (1971). Receptive fields and synaptic organization of the superficial gray layer of the cat
1522 superior colliculus. *Vision Research* 11, 309–IN47. doi:10.1016/0042-6989(71)90048-4
- 1523 Tabareau, N., Bennequin, D., Berthoz, A., Slotine, J.-J., and Girard, B. (2007). Geometry of the superior
1524 colliculus mapping and efficient oculomotor computation. *Biological cybernetics* 97, 279–292
- 1525 Takagi, M., Zee, D. S., and Tamargo, R. J. (1998). Effects of Lesions of the Oculomotor Vermis on Eye
1526 Movements in Primate: Saccades. *Journal of Neurophysiology* 80, 1911
- 1527 Talbot, S. and Marshall, W. (1941). Physiological Studies on Neural Mechanisms of Visual Localization
1528 and Discrimination*. *American Journal of Ophthalmology* 24, 1255–1264. doi:10.1016/S0002-9394(41)
1529 91363-6
- 1530 Tehovnik, E. J., Sommer, M. A., Chou, I.-H., Slocum, W. M., and Schiller, P. H. (2000). Eye fields in the
1531 frontal lobes of primates. *Brain Research Reviews* 32, 413–448. doi:10.1016/S0165-0173(99)00092-2
- 1532 Thelen, D. G. (2003). Adjustment of Muscle Mechanics Model Parameters to Simulate Dynamic
1533 Contractions in Older Adults. *Journal of Biomechanical Engineering* 125, 70. doi:10.1115/1.1531112
- 1534 Thivierge, J.-P. and Marcus, G. F. (2007). The topographic brain: from neural connectivity to cognition.
1535 *Trends in Neurosciences* 30, 251–259. doi:10.1016/j.tins.2007.04.004
- 1536 Thompson, K. G. and Bichot, N. P. (2005). A visual salience map in the primate frontal eye field. In
1537 *Progress in Brain Research*, eds. J. van Pelt, M. Kamermans, C. N. Levelt, A. van Ooyen, G. J. A.
1538 Ramakers, and P. R. Roelfsema (Elsevier), vol. 147 of *Development, Dynamics and Pathology of
1539 Neuronal Networks: from Molecules to Functional Circuits*. 249–262
- 1540 Thompson, K. G., Bichot, N. P., and Sato, T. R. (2005). Frontal eye field activity before visual search errors
1541 reveals the integration of bottom-up and top-down salience. *Journal of Neurophysiology* 93, 337–351
- 1542 Thurat, C., NGuyen, S., and Girard, B. (2015). Biomimetic race model of the loop between the superior
1543 colliculus and the basal ganglia: Subcortical selection of saccade targets. *Neural Networks* 67, 54–73.
1544 doi:10.1016/j.neunet.2015.02.004
- 1545 Tipper, S. P., Howard, L. A., and Paul, M. A. (2001). Reaching affects saccade trajectories. *Experimental
1546 Brain Research* 136, 241–249
- 1547 Ungerleider, L. G. and Mishkin, M. (1982). Two cortical visual systems. In *Analysis of Visual Behavior*,
1548 eds. D. J. Ingle, A. M. Goodale, and R. J. W. Mansfield (Cambridge, MA: MIT Press). 549–586
- 1549 Van Gisbergen, J., Van Opstal, A., and Tax, A. (1987). Collicular ensemble coding of saccades based on
1550 vector summation. *Neuroscience* 21, 541–555. doi:10.1016/0306-4522(87)90140-0
- 1551 Van Gisbergen, J. A. M., Van Opstal, A. J., and Schoenmakers, J. J. M. (1985). Experimental test of two
1552 models for the generation of oblique saccades. *Experimental brain research* 57, 321–336
- 1553 van Opstal, A. J. and Goossens, H. H. L. M. (2008). Linear ensemble-coding in midbrain superior colliculus
1554 specifies the saccade kinematics. *Biological Cybernetics* 98, 561–577. doi:10.1007/s00422-008-0219-z
- 1555 Van Opstal, A. J., Hepp, K., Hess, B. J., Straumann, D., and Henn, V. (1991). Two-rather than three-
1556 dimensional representation of saccades in monkey superior colliculus. *Science* 252, 1313–1315
- 1557 van Opstal, A. J. and van Gisbergen, J. A. (1990). Role of monkey superior colliculus in saccade averaging.
1558 *Experimental Brain Research* 79, 143–149
- 1559 Vokoun, C. R., Huang, X., Jackson, M. B., and Basso, M. A. (2014). Response Normalization in the
1560 Superficial Layers of the Superior Colliculus as a Possible Mechanism for Saccadic Averaging. *Journal
1561 of Neuroscience* 34, 7976–7987. doi:10.1523/JNEUROSCI.3022-13.2014

- 1562 Vokoun, C. R., Jackson, M. B., and Basso, M. A. (2010). Intralaminar and Interlaminar Activity within the
1563 Rodent Superior Colliculus Visualized with Voltage Imaging. *Journal of Neuroscience* 30, 10667–10682.
1564 doi:10.1523/JNEUROSCI.1387-10.2010
- 1565 Vokoun, C. R., Jackson, M. B., and Basso, M. A. (2011). Circuit dynamics of the superior colliculus
1566 revealed by in vitro voltage imaging: Vokoun et al. *Annals of the New York Academy of Sciences* 1233,
1567 41–47. doi:10.1111/j.1749-6632.2011.06166.x
- 1568 Waitzman, D. M., Ma, T. P., Optican, L. M., and Wurtz, R. H. (1991). Superior colliculus neurons mediate
1569 the dynamic characteristics of saccades. *Journal of Neurophysiology* 66, 1716–1737
- 1570 Walker, R., Deubel, H., Schneider, W. X., and Findlay, J. M. (1997). Effect of remote distractors on saccade
1571 programming: evidence for an extended fixation zone. *Journal of neurophysiology* 78, 1108–1119
- 1572 Wickens, J. (1997). Basal ganglia: structure and computations. *Network: Computation in Neural Systems*
1573 8, 77–109
- 1574 Wilson, C. and Kawaguchi, Y. (1996). The origins of the two-state spontaneous membrane potential
1575 fluctuations of neostriatal spiny neurons. *The Journal of Neuroscience* 16, 2397–2410
- 1576 Wilson, C. J. (2004). A Model of Reverse Spike Frequency Adaptation and Repetitive Firing of Subthalamic
1577 Nucleus Neurons. *Journal of Neurophysiology* 91, 1963–1980. doi:10.1152/jn.00924.2003
- 1578 Wu, H. H., Williams, C. V., and McLon, S. C. (1994). Involvement of nitric oxide in the elimination
1579 of a transient retinotectal projection in development. *SCIENCE-NEW YORK THEN WASHINGTON-*,
1580 1593–1593
- 1581 Wurtz, R. H. and Albano, J. E. (1980). Visual-motor function of the primate superior colliculus. *Annual
1582 review of Neuroscience* 3, 189–226. doi:10.1146/annurev.ne.03.030180.001201
- 1583 Wurtz, R. H. and Goldberg, M. E. (1972). Activity of superior colliculus in behaving monkey. III. Cells
1584 discharging before eye movements. *J Neurophysiol* 35, 575–586
- 1585 Yu, J., Tan, M., Wang, S., and Chen, E. (2004). Development of a biomimetic robotic fish and its control
1586 algorithm. *IEEE Transactions on System, Man and Cybernetics - Part B* 34, 1798–1810

FIGURES

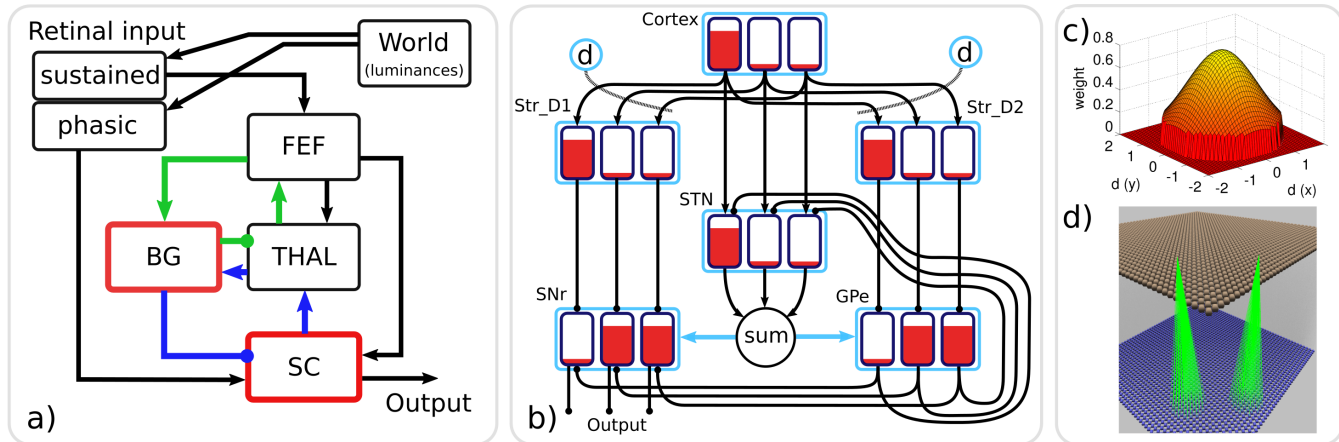


Figure 1. a) The macroscopic architecture of the Cope-Chambers model. The main nuclei modelled as brain systems are: basal ganglia (BG), frontal eye fields (FEF), thalamus (THAL) and superior colliculus (SC). The retinal input is presented via non-biologically plausible retinal populations. The loops through basal ganglia, which define the architecture, are shown with coloured lines: the cortical loop (through FEF and THAL) in green and the sub-cortical loop (through SC and THAL) in blue. Connections with arrowheads indicate excitatory connections, those with circles are inhibitory. A red border indicates that the box represents a sub-system of two or more populations; a black box indicates (at least, within the context of the model) a single neural population. The BG box is expanded in: **b) The basal ganglia model component.** This shows a basal ganglia comprising striatum (Str_D1 & Str_D2), substantia nigra reticulata (SNr). The model has three action channels shown as black boxes within each blue population border. Three channels of cortical input to the BG are also depicted. Red indicates the activation level of a given channel, helping to illustrate the selection mechanism. For example, the channel indicated by the leftmost bar has a high salience (cortical input) and excites activity in Str_D1 which then inhibits the leftmost bar in SNr. The diffuse projection from STN is equivalent to summing its projections channel-wise, and then projecting the sum to all channels of its target populations (the blue arrows indicate that all channels of GPe and SNr are targeted by the connection). Dopaminergic modulation of the inputs to the striatum are indicated by the blue circles labelled 'd' and the dotted lines. The SNr sends inhibitory output projections to its targets. **c) 2D Gaussian weights.** The 'GaussianKernel' connectivity pattern is based on the 'in-plane displacement' between the location of a neural element in one layer, and the location of a target neural element in the target layer for the connection. The potential weight of the connection is given by a 2D Gaussian function, which is maximum for the target neuron which exactly corresponds to the source neuron, and drops down for target neurons which are horizontally displaced from the source neuron. A threshold is applied to avoid a computationally expensive all-to-all connectivity (with most of these connections having negligible weight values). If the weight is non-zero, then a connection is made from source to target, otherwise no connection is made. **d) Gaussian connectivity.** This image shows connectivity (green rays) from two source neurons (in Str_D2, brown spheres) to target neurons (in GPe, blue spheres). The circular connectivity pattern is seen. This does not show the weight values, which reduce 'towards the edge of the circle' and follow the relationship shown in (c).

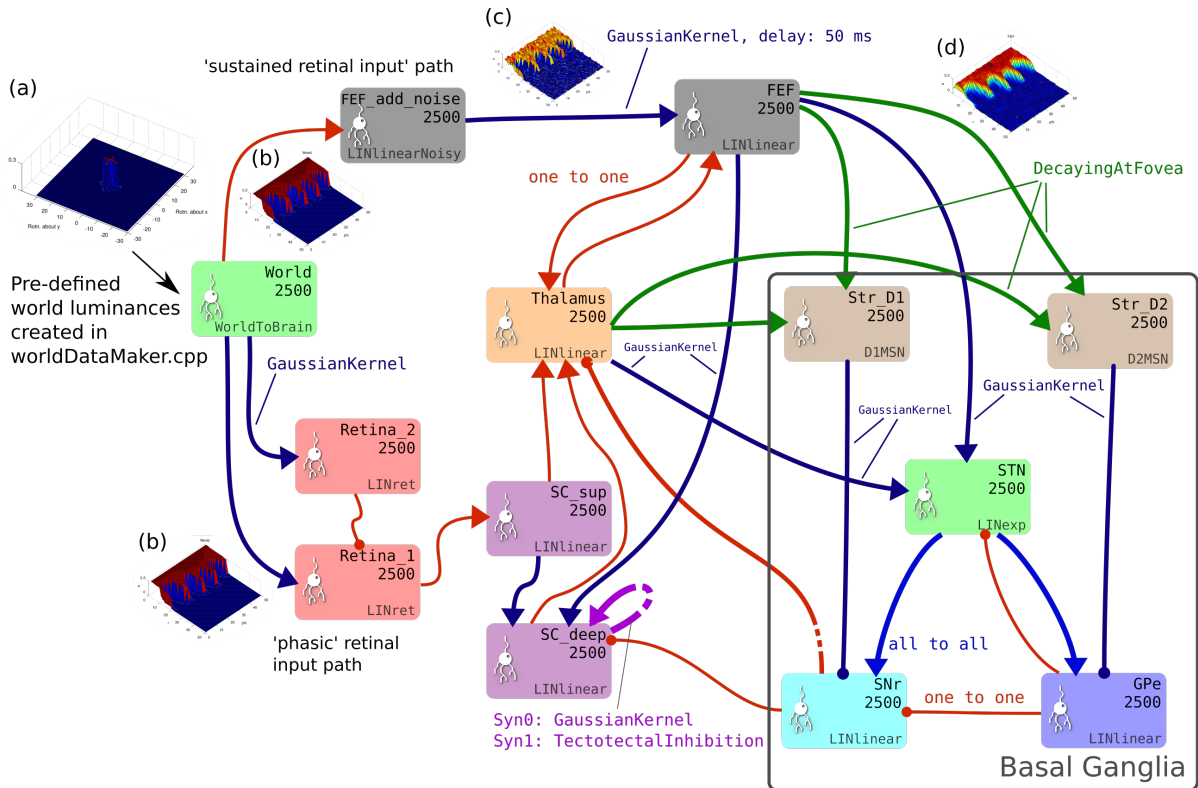


Figure 2. The brain model. This is the SpineCreator ‘network layer’ view of the model. Each box represents a neural population with 2500 elements, arranged in a 50×50 grid. The SpineML component name is printed on the bottom right corner of each population box and the population name is at the top. The overall connectivity between populations is represented by the projection arrows with the colour indicating the connectivity scheme (one-to-one connections are red, Gaussian kernel connections are dark blue and so on). Excitatory connections have arrowheads and inhibitory connections have circles, although for details of the behaviour of the connections, the weight-update and post-synapse components must be studied. Briefly, the model comprises a *World* population, into which a retinotopically organised view of the world is introduced. This information is passed into cortical populations (FEF) and subcortical populations (SC) via a simple model of the retina. These feed a cortico-thalamo-basal ganglia loop, which selects which region of the deep layer of superior colliculus should be disinhibited, allowing activity to build up therein. The five populations comprising the basal ganglia are enclosed in a grey outline. Note that substantia nigra pars compacta is not modelled here, instead the level of dopamine in the striatum is set via a parameter in the Str.D1 and Str.D2 populations

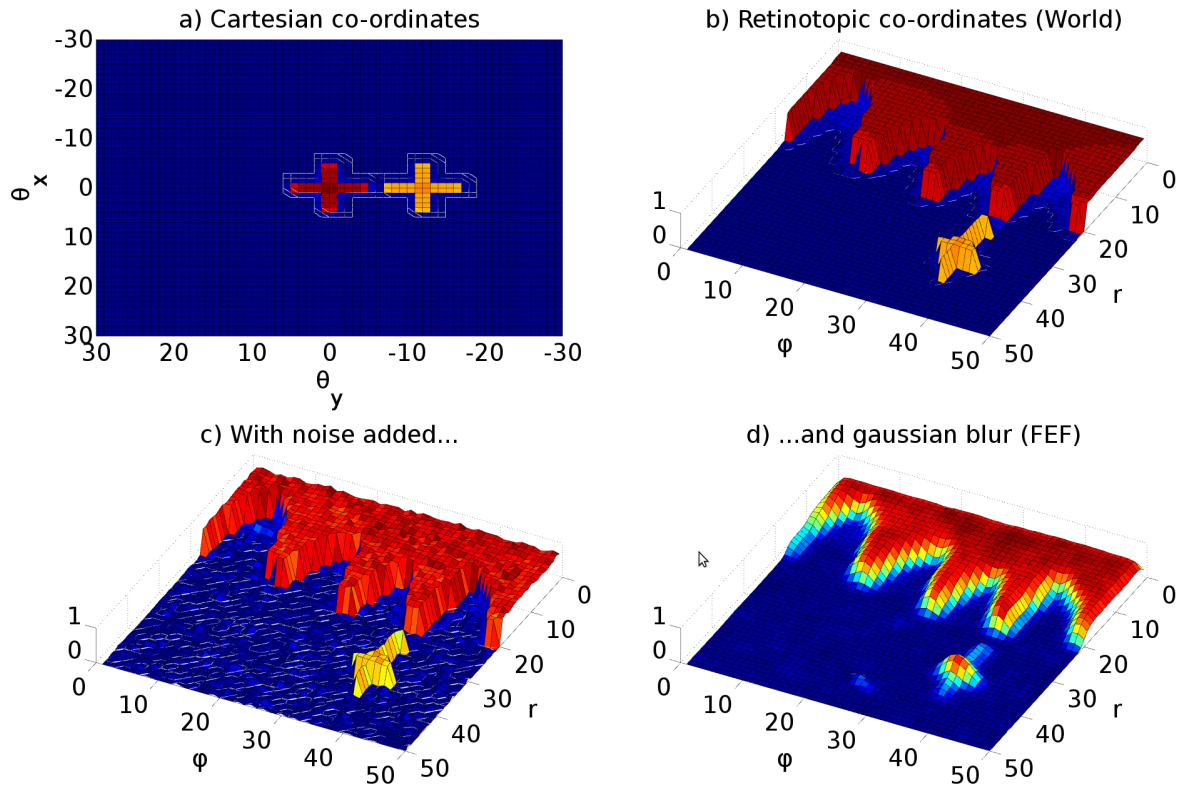


Figure 3. Representative mapping from eye's frame of reference in Cartesian co-ordinates to retinotopic co-ordinates. (a) The mapping of luminances in the eye's frame of reference. The world input is pre-defined by a JSON configuration file. Luminance position, size and shape can be defined in this file, along with the times at which luminances appear and disappear. The `worldDataMaker.cpp` code computes the locations of the luminances in the eye's frame of reference, given its rotational state. It also computes a 2D Gaussian convolution of the luminances. Here, there are two cross shaped luminances spanning 10° , one of value 0.8 at the fixation point (0,0) and one of value 0.5 at a peripheral position (0,-12°). Note that these crosses have the same 'bar width' of 2° as the crosses used in the simulations, but their span of 10° is greater than the 6° used in the simulations, to make these images clearer. (b) The locations of the luminances in the eye's frame of reference are then converted into retinotopic co-ordinates, with centrally located luminances being represented at low values of r and more peripheral luminances having higher values of r . ϕ encodes rotational angle: 1 and 50 encode upward movement; 13 is left; 25 is down; 37 is right. The output of the World component is fed into `FEF_add_noise` and into the retinal neuron populations. The colour map makes it possible to distinguish between the two crosses. (c) The `FEF_add_noise` populations adds a level of noise to the signal representing processing of the signal in visual cortex. (d) A Gaussian projection from `FEF_add_noise` to FEF further blurs the activity in FEF. FEF is the input to the basal ganglia and one input to superior colliculus.

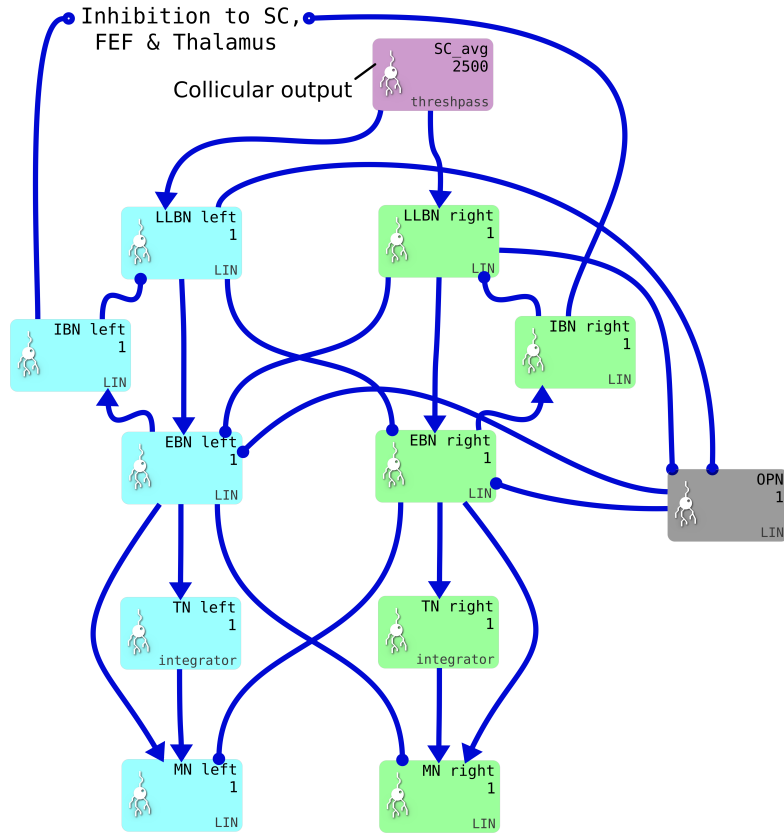


Figure 4. One pair of channels of the saccadic burst generator (SBG) for left (cyan) or right (green) movements. Collicular activity in SC_avg excites the channels via SBG weight maps. Each box represents a neural population and shows the population name, the number of neural elements (here 2500 or 1) and the SpineML component name; LIN for Leaky integrator or *integrator*. Key: LLBN: Long lead burst neurons; IBN: Inhibitory burst neurons; OPN: Omnipause neurons; EBN: Excitatory burst neurons; TN: Tonic neurons; MN: Motoneurons.

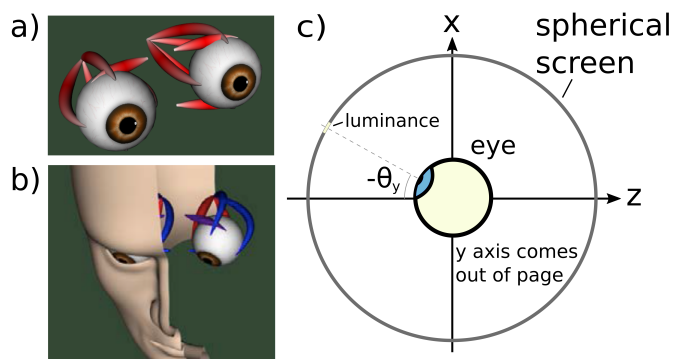


Figure 5. The biomechanical eye. a) an OpenSim rendering of a pair of biomechanical eyes showing the positions of the extraocular muscles. Note that i) volume visualization of muscles should not be confused with FEM muscle models; it is provided for user feedback purposes, i.e. shape and color change depending on the muscle activation, ii) superior and inferior oblique are visualized up to their respective muscle pulleys. b) OpenSim rendering of biomechanical eye within a head model c) Top-down schematic cross-sectional view of the biomechanical eye situated within a spherical screen, with a horizontal rotation towards luminances at an angle of $-\theta_y$ about the y axis. The y axis points up, out of the page.

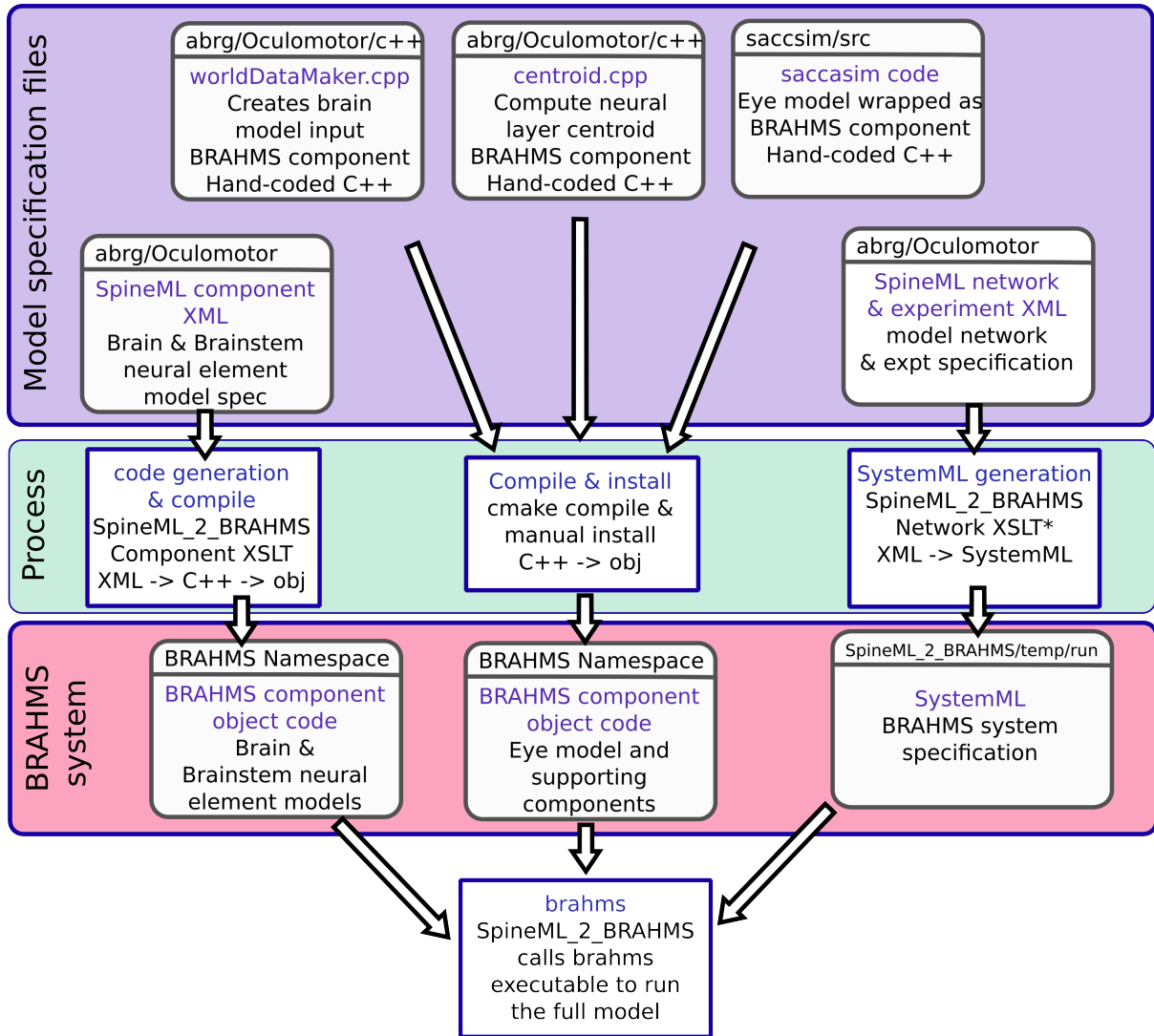


Figure 6. The model framework. The model is specified using a combination of declarative XML files and hand-coded C++. These original model specifications are shown within the blue box. b) The green box shows the processes which are applied to the model specification to produce the BRAHMS system. Most of the process is defined within the scripts which make up SpineML_2_BRAHMS, but the hand-written components must be manually compiled and installed within the BRAHMS Namespace, allowing the BRAHMS executable to locate them at runtime. c) The red box shows the resulting BRAHMS system ready to be executed by the BRAHMS executable. In practice, this call is made by SpineML_2_BRAHMS.

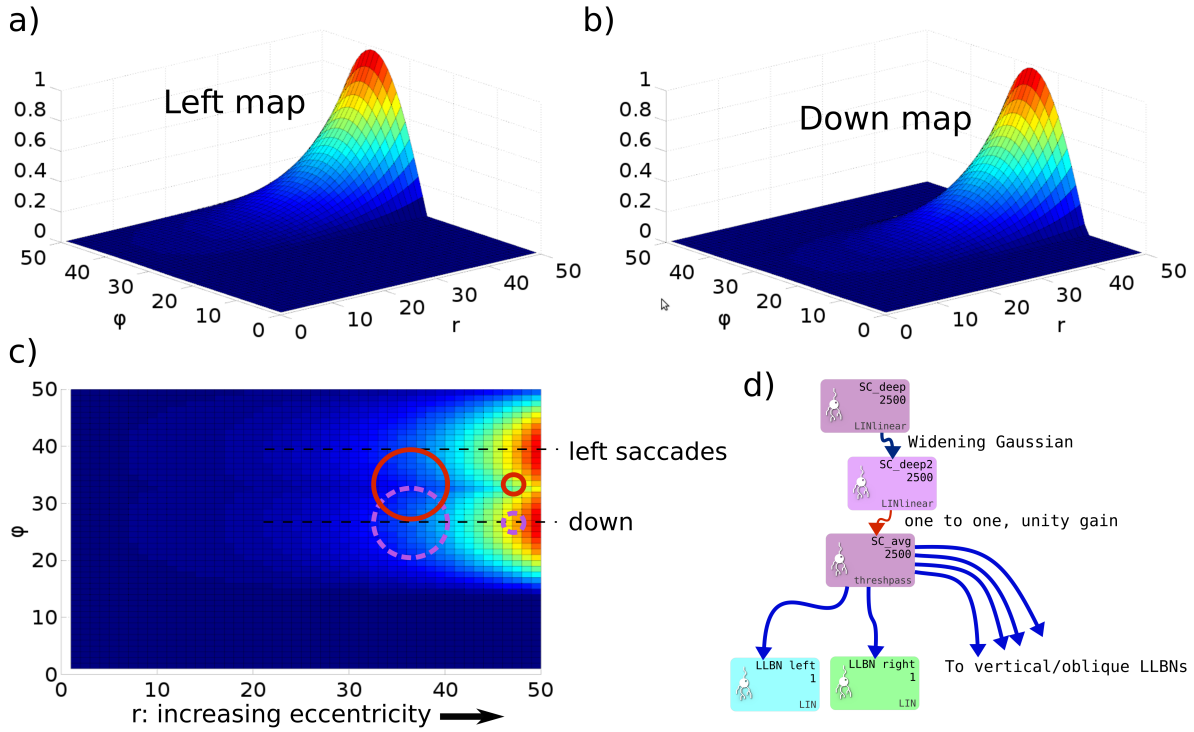


Figure 7. a) & b) Tabareau-style weight maps for ‘left’ and ‘down’ components of a saccade. c) The two weight maps in a) and b) shown on the same graph, viewed from above. Circles show the locations of potential hills of activity. Purple, dashed circles encode saccades down; red circles encode saccades with both a left and a down component. d) Showing the additional deep layer of superior colliculus (SC_deep2) and the output layer (SC_avg, named for the fact that in an earlier version of the model, it received the output of the centroid of SC_deep). The widening Gaussian projection is shown as the arrow between SC_deep and SC_deep2.

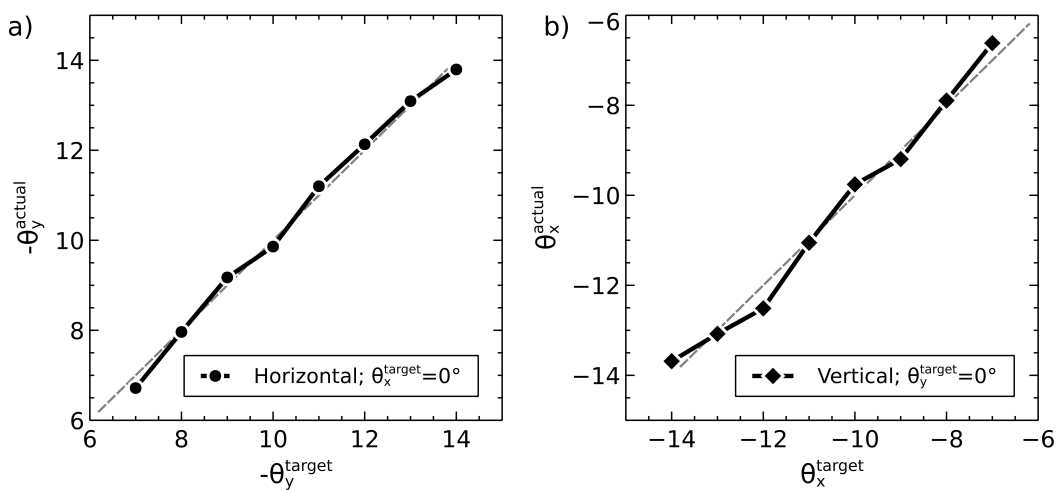


Figure 8. Accuracy at different target eccentricities for fixation luminance 0.2 and target luminance 0.3.

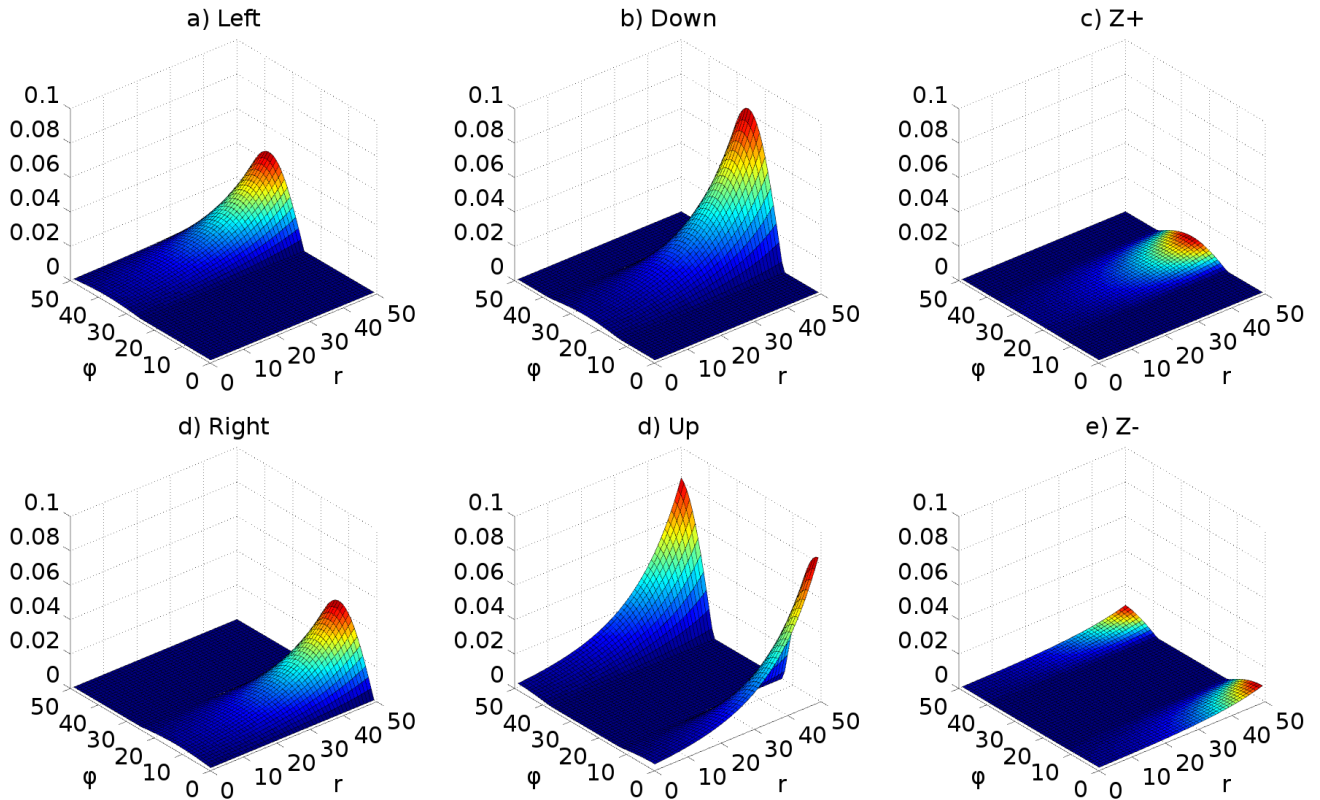


Figure 9. Weight maps for the connections between the output layer of superior colliculus and the six long lead burst neurons of the saccadic burst generator model. Each map increases exponentially with increasing r , multiplied by $\cos(\phi)$ about its ‘active’ axis.

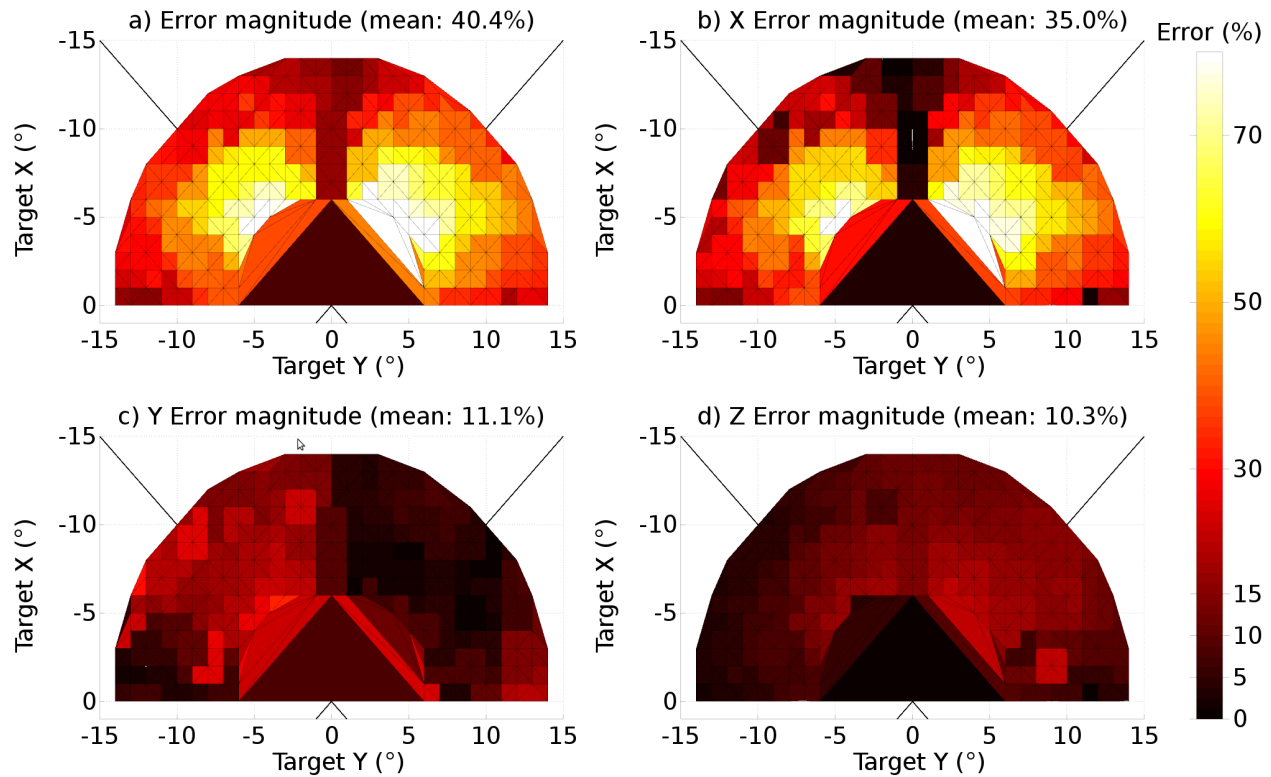


Figure 10. The end-point error surface for the original, naïve model (TModel3). a) The ratio of the magnitudes of the total error vector and the target vector, expressed as a percentage. b) The ratio of the magnitude of the x component of the error vector to the magnitude of the target vector, expressed as a percentage. c) As (b) but for the y component. d) As (b), for z component. All colour maps are shown with the same scale. The target rotations, θ_x^t and θ_y^t are denoted ‘Target X’ and ‘Target Y’ in the figure.

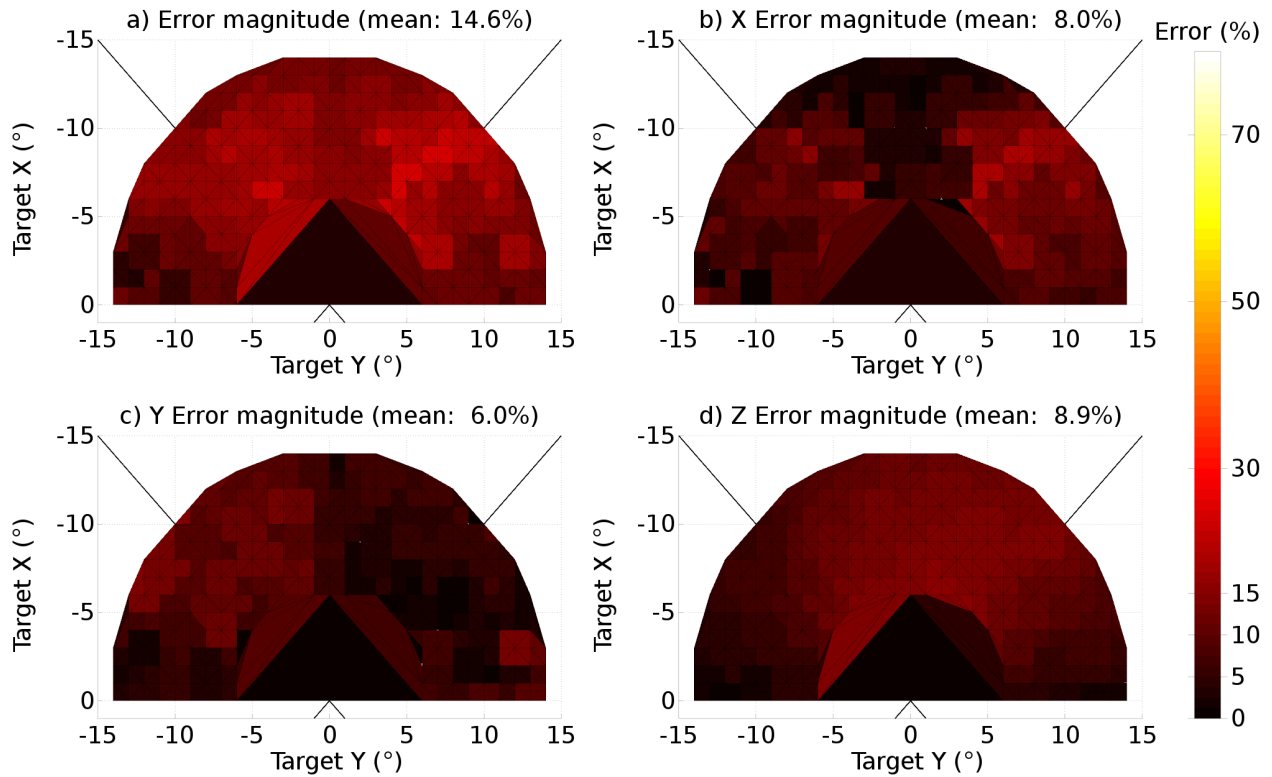


Figure 11. The end-point error surface for the model in which a widening projection field was added to the model of the superior colliculus. a) The ratio of the magnitudes of the total error vector and the target vector, expressed as a percentage. b) The ratio of the magnitude of the x component of the error vector to the magnitude of the target vector, expressed as a percentage. c) As (b) but for the y component. d) As (b), for z component. All colour maps are shown with the same scale. The target rotations, θ_x^t and θ_y^t are denoted ‘Target X’ and ‘Target Y’ in the figure. Note that the range of the colour scale is 0 to 20%, a much smaller range than the range in Fig 10.

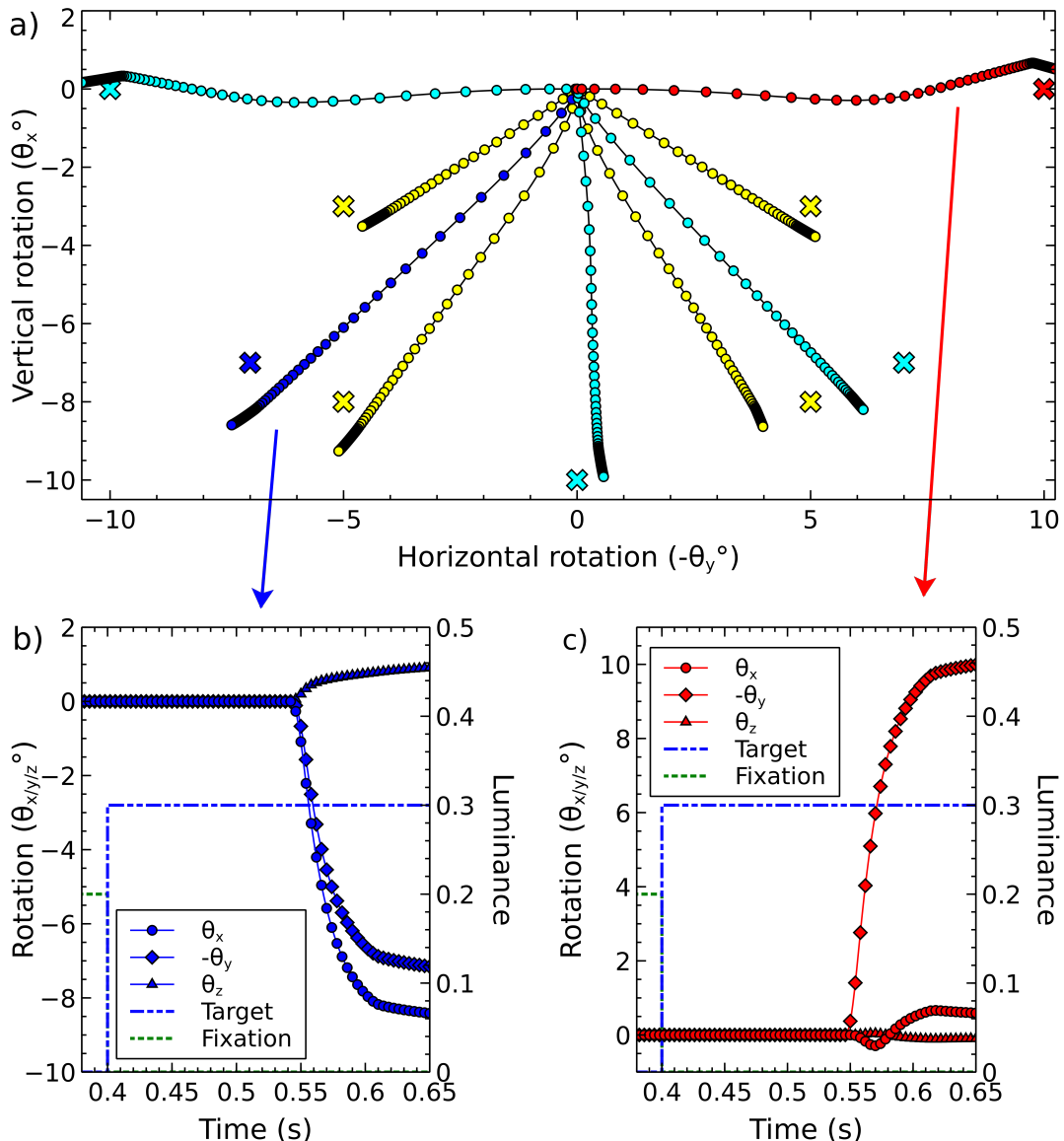


Figure 12. Representative single saccades. a) Trajectories from 9 saccades to a single target at 9 different locations. In each case, a fixation cross luminance of magnitude 0.2 was displayed at (0,0), the start position of the eye, until time 0.4 s. The target luminance, magnitude 0.3 was illuminated at time 0.4 s. Trajectory shape is dependent on the target position, and there is a variable amount of error in the end-points achieved by the model. Colour is used in this diagram as an aid to distinguishing different saccades and their targets; for a given saccade, the target location is given by the cross of the same colour closest to the end of the trajectory. b) The three rotational components of the ‘blue’ saccade, to target location (-7,-7). c) The three rotational components of the ‘red’ saccade, to target location (0,-10).

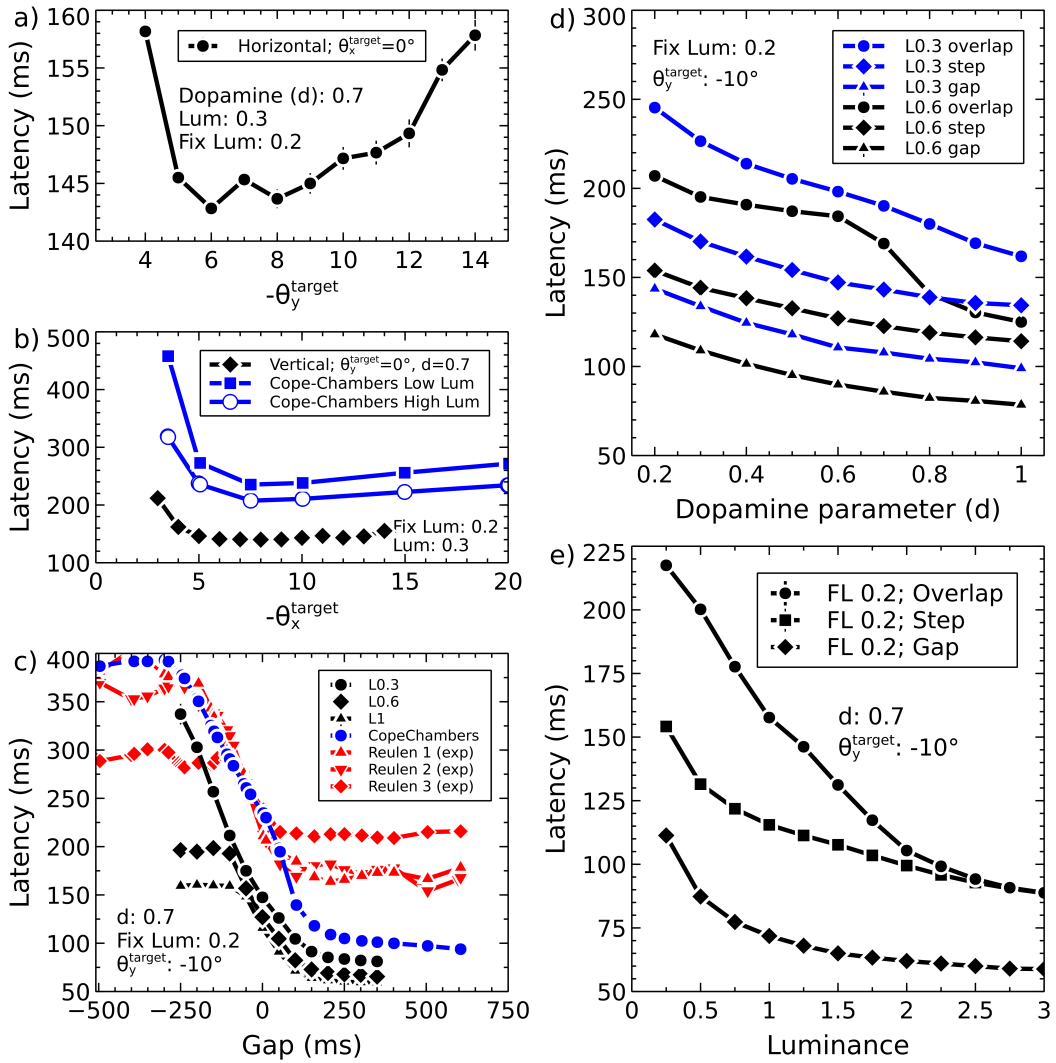


Figure 13. Exploring saccade latencies. a) Latency to first movement as a function of target eccentricity for horizontal targets. b) Latency vs. eccentricity for vertical targets. c) Latency vs. gap at three different luminance values. The data are shown alongside the Cope-Chambers model results from Fig. 5 of Cope et al. (2017) in blue, and the experimental results used in that model in red. The fixation luminance for the Cope-Chambers curve was 0.5, the target luminance 0.6 and the target eccentricity was 8° . The difference between the Cope-Chambers model data and the data from the current model results from the different mechanism by which activity in SC_deep causes a movement, the differing target angle and the reduced fixation luminance used here. d) The effect of the dopamine parameter on saccade latencies in gap, step and overlap conditions, for two different target luminances. e) Saccade vs. luminance showing gradual transition between reflexive and express behaviour.

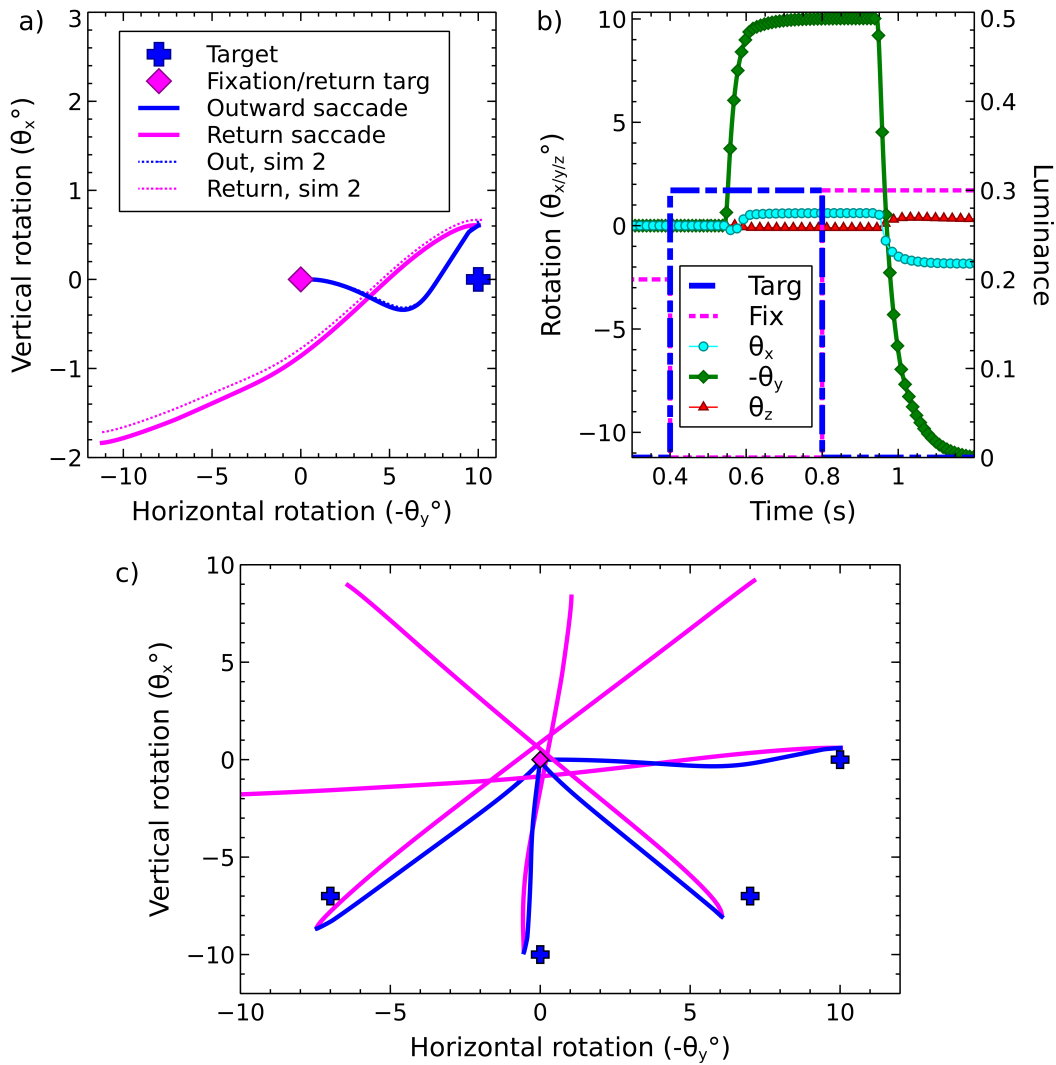


Figure 14. There and back - a saccade to a target, followed by return to the original fixation. a) Out and return saccade to a target at $(0, -10^\circ)$ b) Rotational components of the saccade shown in (a). c) Outward and return trajectories for the saccade shown in (a) alongside saccades to three other targets.

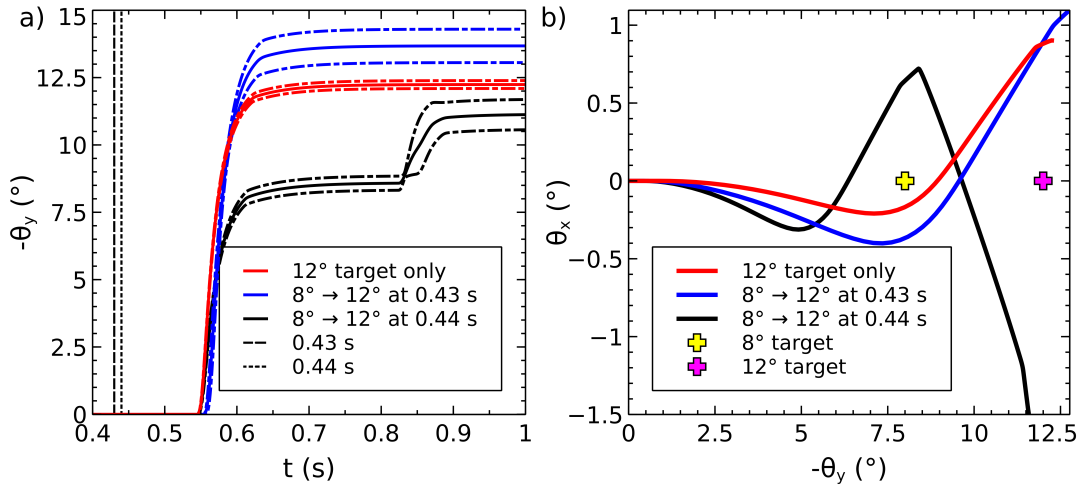


Figure 15. Double steps. The effect of illuminating a first target at 8° or 12° , followed by a second target at 12° or 8° . a) Horizontal rotation of the eye plotted vs. time for a saccade to the 12° target only (red), and to an 8° target at 0.4 s followed by a 12° target after 30 ms (blue) or 40 ms (black). The timings are indicated by vertical lines. When the second target is presented up to 30 ms after the initial target, the initial target has not had time to dominate the output saccade and a saccade to a location close to the second target is made. If the delay is 40 ms or more, the activity from the initial target has time to cause a built up of activity in SC_deep and an initial saccade close to the first target is made, followed, after a longer than usual latency period, with a second saccade closer to the second target. In this graph, the mean of five separate simulations is plotted along with ± 1 standard deviation around the mean. b) The θ_x/θ_y trajectories corresponding to the data presented in (a).